Department of Mechanical Engineering
TUM School of Engineering and Design
Technical University of Munich

Modeling of Convective Heat Transfer in Automotive Headlamps

For Simulation-based Design

Scientific work for obtaining the academic degree

Bachelor of Science (B.Sc.)

at the TUM School of Engineering and Design of the Technical University of Munich

Supervisor Hon.-Prof. Dr.-Ing. Martin Otter

Advisor Dr. Sebastian Bartscher
Ing. Andreas Lintz

Submitted by Jesus Gabriel Virto Chirhuana

Submitted on July 01, 2024 in Garching

Abstract

LED technology is continuously replacing conventional lamps in many technical applications, including headlights. The advantages are numerous because LEDs offer high energy efficiency, a compact size, a long lifetime and the potential for innovative headlamp designs. However, a disadvantage is that LED components tend to react very sensitively to heat, affecting the performance of the light and its lifetime. Therefore, an optimized thermal management system inside headlamps is always required for adequate cooling of the light modules in order to prevent LED failures. Because of these reasons, in this work, 1D modeling will be developed to represent the heat transfer processes inside a headlamp in order to get an accurate prediction of the LED temperature. This thesis introduces a library with the implementation of thermo-fluid components, which will help describe the convective transfer mechanism and the airflow behavior. In the early stages of the development phase, it is necessary to decide which headlamp designs have more potential for further development, fulfilling the customer requirements. The first task is to study thermal theory and fluid dynamic concepts, whose analytical approaches are implemented in the modeling. The results from the 1D modeling will be compared to previously conducted CFD simulations of the same headlamps in order to evaluate the accuracy of the temperature results.

Zusammenfassung

Die LED-Technologie ersetzt kontinuierlich herkömmliche Lampen in vielen technischen Anwendungen, einschließlich Scheinwerfern. Die Vorteile sind zahlreich, da LEDs hohe Energieeffizienz, kompakte Größe, lange Lebensdauer und das Potenzial für innovative Scheinwerferdesigns bieten. Ein Nachteil ist jedoch, dass LED-Komponenten sehr empfindlich auf Hitze reagieren, was sich auf die Lichstärke und die Lebensdauer auswirkt. Daher ist ein optimiertes thermisches System in den Scheinwerfern immer erforderlich, um eine richtige Kühlung der Lichtmodule zu gewährleisten und LED-Ausfälle zu verhindern. In dieser Arbeit wird ein 1D vereinfachtes Modell entwickelt, um die Wärmeübertragungsprozesse innerhalb eines Scheinwerfers darzustellen, um eine genaue Vorhersage der LED-Temperatur zu erhalten. Diese Arbeit führt eine Bibliothek mit der Implementierung von Thermo-Fluid-Komponenten ein, die helfen wird, die konvektive Wärmeübetragung und das Strömungsverhalten der Luft zu beschreiben. In den frühen Phasen der Entwicklung ist es notwendig zu entscheiden, welche Scheinwerferdesigns das meiste Potenzial für die weitere Entwicklung haben, um die Kundenanforderungen zu erfüllen. Die erste Aufgabe besteht darin, die Wärmetheorie und die fluiddynamischen Konzepte zu studieren, deren analytische Ansätze in der Modellierung umgesetzt werden. Die Ergebnisse der Simulation werden mit zuvor durchgeführten CFD-Simulationen derselben Scheinwerfer verglichen, um die Genauigkeit der Temperaturergebnisse zu bewerten.

Contents

List of Figures

List of Tables

List of Abbreviations

1D One-dimensional

3D Three-dimensional

CAD Computer Aided Design

CFD Computational Fluid Dynamics

DCC Double Climate Chamber

GUI Graphical User Interface

HL Headlamp

HS Heat Sink

IC Integrated Circuit

LED Light Emitting Diode

LM Light Module

OSMC Open Source Modelica Consortium

PCB Printed Circuit Board

SCC Single Climate Chamber

Nomenclature

Symbols

α	Heat transfer coefficient
α_f	Thermal diffusivity of the fluid
β	Thermal expansion coefficient
ΔP	Pressure drop
ΔT	Temperature difference
$\dot{H}$	Enthalpy flow rate
$\dot{V}$	Volume flow rate
η	Heat sink fin efficiency
μ	Dynamic viscosity
ν	Kinematic viscosity
ρ	Density
σ	Stefan-Boltzmann constant
ε	Emissivity of the surface
A	Surface area
c_p	Specific heat capacity
C_{th}	Heat capacity
d	Thickness of the solid
g	Gravitation constant
h	Specific enthalpy
k	Thermal conductivity
k_f	Thermal conductivity of the fluid
m	Mass of the solid
P_{th}	Thermal power loss
R_{th}	Thermal resistance

T	Temperature
u	Velocity of the fluid
V_{ch}	Air average velocity in the heat sink channel

Dimensionless numbers

Gr	Grashof number
Nu	Nusselt number
Pr	Prandtl number
Ra	Rayleigh number
Re	Reynolds number

Chapter 1

Introduction

1.1 Motivation

Vehicles remain relevant for mobility and economic activity. Headlamps are essential in the automotive lighting system not only for the light functions that offer elevated safety and driving experience through optimal road illumination and signaling but also represent a relevant part of the car's appearance. Headlamp performance and appearance are important requirements for customers demanding the latest technology and new styling characteristics. The current automotive lighting state-of-the-art relies on LED light sources due to their advantages, e.g., their superior efficiency and lifetime, over conventional lighting systems such as halogen or xenon headlamps.

This work focuses on two pivotal challenges that need to be considered in the process of developing new headlamp designs: thermal optimization and defogging process. The first of those challenges is the thermal management system inside headlamps, which affects the performance of the light module because the LED components tend to react very sensitively to heat. The other challenge is avoiding condensation on the external cover lens, which limits the headlamp's illumination and affects its visual appearance.

Inside and outside headlamps have different heat sources, e.g., the light function, the engine's heat, and ambient temperatures, altering the internal air temperature. At elevated operating temperatures, based on poor design and quality of the heat management system, the main consequence is a reduction in LED lifetime and luminous efficacy. See Figure 1.1, where those characteristics suffer negative effects on performance over time at different temperatures.

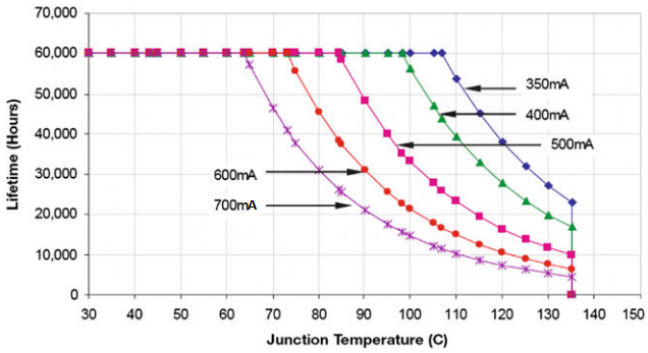

Figure 1.1: Lifetimes for AlInGaP LED [1]

An undesirable fogging and defogging process on the cover lens happens due to the presence of humidity within the headlamp when an abrupt temperature drop occurs. Water condensation on visible parts

is a negative aspect of the headlamp's appearance and impact on the light functionality, as illustrated in Figure 1.2.

Figure 1.2: Condensation has taken place on the headlamp's outer lens [2]

Therefore, knowing that high temperatures are a concern for performance and appearance, an efficient thermal management system is always required. For this condition, suitable heat sinks are always necessary, and sometimes, a fan is needed to ensure appropriate cooling of the LED module. Both active and passive cooling concepts rely on air movements inside the headlamp.

Modeling the thermal system is a crucial step in studying and analyzing the thermal transfer and airflow behavior inside the headlamp. The reason for knowing the temperature data through simulations is to find improvements for the cooling system, prevent future failures of the LED module and predict the de-/fogging behavior.

1.2 Relevance of Simulations

In the past decades, the automotive headlamp development process has relied chiefly on physical tests, where the construction and geometry need multiple revisions until satisfactory results are achieved. This approach is both costly and time-consuming because it involves tests in climate chambers and light tunnels in order to validate the newly designed headlamp [2]. However, these costs can be reduced by using numerical simulations of headlamps before sending them to production. Figure 1.3 below illustrates that the possibility of modifying the headlamp decreases over time, while the costs of these alterations escalate with time.

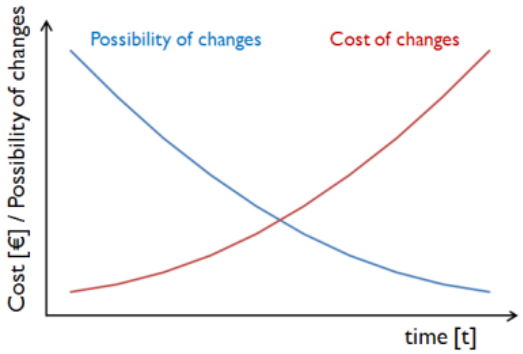

Figure 1.3: Possibility of making changes versus the cost of changes in time [2]

Currently, modeling and simulation play a pivotal role in engineering by building complex systems and understanding their behaviors. While new headlamp technology is being developed, the required design must be optimized in terms of quality, cost, and lifetime. To find improvements, the system inside the

headlamp must be analyzed by building a simulation that should be created so that the results can be compared and validated concerning the real-world behavior of that system. See Figure 1.4 for a better understanding of the development process.

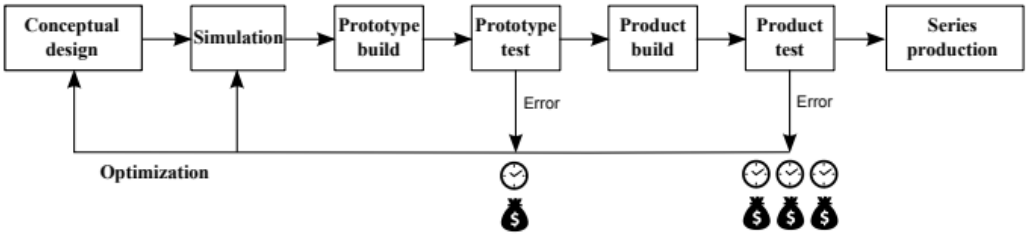

Figure 1.4: Development process of a headlamp nowadays [3]

Nowadays, the automotive industry is using numerical simulations. Computational Fluid Dynamics (CFD) simulations have been implemented to conduct those simulations in the development process, in this case, to predict and optimize the heat transfer and fogging behavior inside headlamps. The CFD process involves three essential steps: Pre-processing, solving and post-processing. In the pre-processing stage, the 3D CAD geometry of the headlamp is imported and cleaned up based on specified details and areas of interest [2]. The necessity of a 3D model leads to a critical challenge in the early developmental period because different data/parameters, such as the final geometry inside the headlight, are unknown in the preliminary designs of headlamps; therefore, it is complicated to build a detailed CAD model and carry out CFD simulations with high accuracy.

Thus, a low-order design/modeling that does not require inputs such as the headlamp's geometry and components' positions might address the lack of a 3D CAD model. Furthermore, in the early design period, faster results are needed to decide which designs are better or have more potential for further development.

1.3 Scope and Goal of the Thesis

In the development of headlights and innovative technologies, the primary objectives are, first, to raise the lifetime of the light module as long as possible and maintain the efficiency of the LED. To achieve these two objectives, it is essential to predict the temperatures to which the LEDs in the headlamp will withstand since the lifetime and efficiency are linked to the junction temperature for the sake of high-quality LED-based products. That prediction of the temperature data is the main reason for developing a model that accurately represents the thermal management of the headlight.

This work aims to develop and validate a model of heat convection within the software OpenModelica. The principal objective is integrating the convective heat transfer process inside a headlamp. An innovative aspect of this work is to do the entire modeling with the modeling language Modelica using OpenModelica. This thesis should answer how accurately the Modelica model predicts temperature changes in realistic headlamp designs, including heat sinks, fans and PCBs. It is essential to evaluate the suitable approaches, the required inputs, and their specifications.

The challenge is to find a suitable way to implement convective heat transfer and air movement in a thermal system with adequate accuracy. The model might be used to assist CFD simulations. However, the purpose is for the model to be sufficient for an accurate prediction, i.e., temperature data replacing CFD simulation in early product development.

Chapter 2

Theoretical Background

To properly understand the thermal behavior inside a headlamp, different concepts of physics, especially heat transfer and fluid mechanics, must first be studied. There are heat sources inside and outside the headlamps, such as the light function, engine, and environmental factors, producing temperature differentials that generate a heat transfer process and need to be considered during the development of a headlamp. Also, it is essential to study the movement of air, which acts as a coolant.

2.1 Fundamentals of Heat Transfer

Heat transfer is the fundamental process of exchanging thermal energy between physical systems. Heat is the energy that is transferred due to a temperature difference. For a better understanding of heat transfer and the establishment of its equations, studying the thermodynamic laws is important because the equations in heat transfer are determined by the principles outlined in the first and second laws of thermodynamics.

The first law of thermodynamics, the "principle of energy conservation", says that energy cannot be created or destroyed; it can only change its form. Energy transitions can be represented when one type of energy, like work on a system, is converted to thermal energy [4]. For a closed system, the change in the total energy stored in the system is given by:

$$\Delta E = Q - W \tag{2.1}$$

where Q is the net heat transferred to the system and W is the net work done by the system.

In summary of the thermodynamics laws, the direction of the heat transfer always goes from the higher-temperature level to the lower-temperature one to create equilibrium. The first law of thermodynamics is extensively applied in deriving governing equations for the modes of heat transfer, which are conduction, convection, and radiation [4].

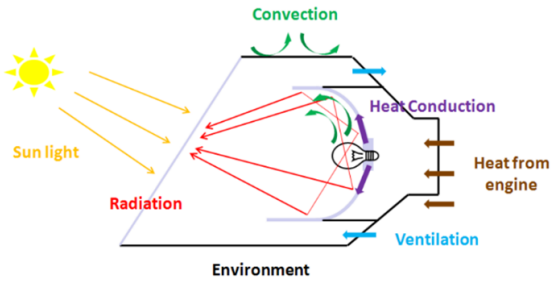

Figure 2.1: Different heat transfer processes in a headlamp [2]

2.1.1 Thermal Conduction

Conduction is the transfer of energy from the more energetic particles of a substance to the less energetic molecules because of particle interactions (microscopic motion). It can occur in a medium such as solids (due to the combination of vibrations of the molecules) or liquids and gases (due to the collisions and diffusion of the molecules during their random motion) [5]. Fourier's law is required to quantify the conduction heat transfer through a flat wall, determined by its geometry, thickness, and material properties, as shown in Figure 2.2.

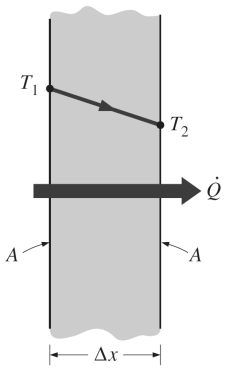

Figure 2.2: Conduction through a flat and homogeneous wall [5]

It is known that the conductive heat flux is proportional to both the temperature difference and the constant thermal conductivity λ, representing a material's ability to transport heat.

$$\dot{Q}_{\text{cond}} = k \cdot A \cdot \frac{\Delta T}{d} = \lambda \cdot A \cdot \frac{(T_1 - T_2)}{d} \tag{2.2}$$

where A is the cross-sectional area through which heat flows, and d is the thickness.

2.1.2 Thermal Convection

Convection is the transfer of heat through the movement of fluids over a solid surface. It relies on the bulk movement of fluid particles to transport heat from one location to another. Figure 2.3 shows that heat is extracted from a heated solid surface to a cooling fluid, presenting a boundary-layer flow and heat transfer scenario [5].

According to Newton's law of cooling, the dissipated heat rate from the surface is proportional to the temperature difference between the heated wall and the cooling fluid, and the proportionality constant is known as the heat transfer coefficient. This relationship is presented in the following equation:

$$\dot{Q}_{\text{conv}} = \alpha \cdot A \cdot \Delta T = \alpha \cdot A \cdot (T_\infty - T_s) \tag{2.3}$$

where α is the convective heat transfer coefficient, A is the surface area through which heat is transferred through which heat flows and ΔT is the temperature difference between the surface and the surrounding fluid.

Natural Convection and Forced Convection

Natural convection is commonly identified as the flow of air prompted by temperature variations and is also referred to as buoyancy-driven flow. When the temperature of the fluid increases, its density decreases, causing the warmed air to ascend while colder air moves in from below to replace it [2]. A classic example is the rising of warm air near a hot surface, which causes the air to ascend, ultimately transferring heat away from the surface.

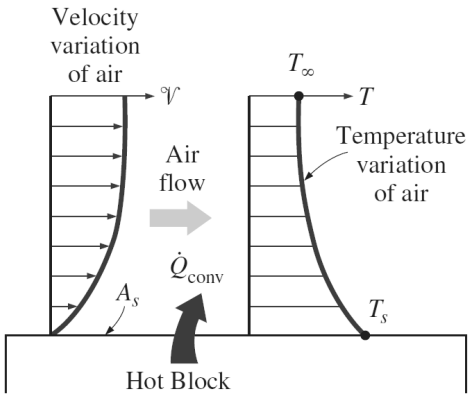

Figure 2.3: Convective heat transfer from hot surface to cold air [5]

Compared to natural convection, forced convection includes an external force or mechanical energy that impels the fluid to move. Some devices, such as fans, pumps or blowers, generate that force, inducing the fluid to a faster motion, allowing an efficient heat transfer. The differences in the airflow can be observed in Figure 2.4. Therefore, the application of forced convection is usually required for cooling, enhancing the value of the heat transfer coefficient in comparison with natural convection.

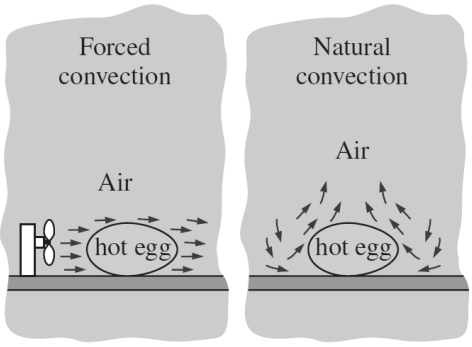

Figure 2.4: Cooling a boiled egg by forced and natural convection [5]

2.1.3 Thermal Radiation

Radiation represents a distinct mode of heat transfer. Unlike conduction and convection, which require a material medium, radiation allows heat to be transferred even through a perfect vacuum [5]. In this scenario, electromagnetic radiation is the transfer mechanism, traveling at the speed of light.

A black body is an idealized surface that radiates at this maximum rate, and the radiation it emits is referred to as black body radiation, as shown in Figure 2.5. Real surfaces emit less radiation than a black body at the same temperature ($\varepsilon = 1$ for a black surface and $\varepsilon < 1$ for a non-black surface). According to Stefan-Boltzmann law, the emission of radiation from a black body is:

$$\dot{Q}_{\text{rad}} = \varepsilon \cdot \sigma \cdot A \cdot T_s^4 \tag{2.4}$$

The thermal radiation, produced due to a temperature difference between heat-exchanging bodies (surface and ambient) [6], is determined by:

$$\dot{Q}_{\text{rad}} = \varepsilon \cdot \sigma \cdot A \cdot (T_s^4 - T_\infty^4) \tag{2.5}$$

where $\dot{Q}_{\text{rad}}$ is the heat transfer rate, σ is the Stefan-Boltzmann constant, A is the surface area of the body, ε is the emissivity of the surface, and T_s and T_∞ are the absolute temperature of the body and the ambient temperature respectively.

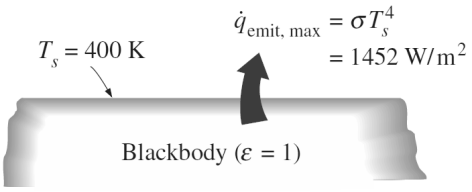

Figure 2.5: Black body radiation [5]

2.2 Fundamentals of Fluid Mechanics

2.2.1 Fluid Parameters

The nature of the fluid is represented by its physical and transport properties. The variation of these properties within the flow domain determines the analysis method. The fluid can be characterized by the following models: incompressible or compressible fluids, non-viscous fluids or viscous fluids, and fluids with constant thermo-physical properties or variable thermo-physical properties [7].

In the case of a headlamp, the fluid to be studied is air, which is a compressible fluid with variable thermo-physical properties. Compressibility is when the fluid's density changes over time due to changes in pressure or temperature. Variable properties such as viscosity and thermal conductivity due to changes in temperature influence the heat transfer coefficient.

2.2.2 Flow Conditions

The nature of the flow may be divided for practical applications, depending on the different flow conditions, such as laminar flow, turbulent flow, natural or forced convection, and mixed convection, where forced and free convection occur simultaneously. Knowing and studying those flow conditions is important because they significantly impact the heat transfer coefficient. The conditions enhance the heat transfer compared to the conduction heat transfer in a solid or stationary fluid.

Laminar and turbulent flows are also represented in the boundary layers. These layers represent the changes or alterations of the free stream values within the layer with a thickness δ. The thermal boundary layer is created near the solid surface when a fluid is flowing over a solid body, transferring heat. In most convective heat transfer cases, laminar and turbulent flow conditions coexist, where the laminar section occurs before the flow becomes turbulent. In the laminar section, the fluid flow is highly organized, allowing faster identification of the fluid streamlines, as shown in Figure 2.6. Conversely, turbulent flow is typically irregular, with random changes of directions and velocities growing the boundary layer thickness. There is a transition zone where a transformation from laminar to turbulent conditions occurs.

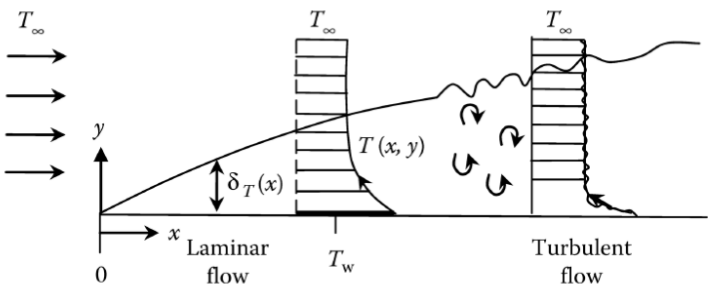

Figure 2.6: Thermal boundary layer [8]

Figure 2.6 shows the temperature distribution when the heat dissipates from a hotter plate to the air (coolant) according to Newton's cooling law. Thus, the fluid temperature increases from its free stream value to the value from the solid surface. It is important to notice that the flow conditions (whether laminar or turbulent flows) impact the heat transfer coefficient, as shown in Figure 2.7. The heat transfer coefficient can be calculated through experimental or analytical approaches.

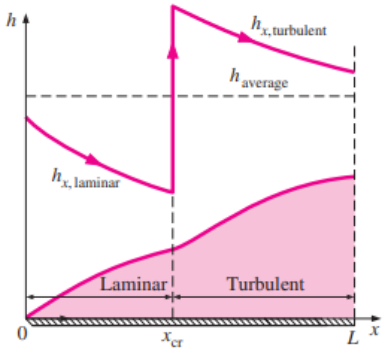

Figure 2.7: Variation of the heat transfer coefficient depending on the flow condition [5]

2.2.3 Dimensionless Numbers

Dimensionless numbers, derived from fundamental physical principles and equations, characterize and compare the behavior of diverse fluid flow phenomena. When discussing analytical approaches to calculate the heat transfer coefficient in order to describe the thermal processes inside and around headlamps, it is important to understand and apply the correct number for each case, depending on airflow conditions.

Prandtl Number

The Prandtl number (Pr) is a fluid property, representing the ratio of momentum transfer versus heat transfer. Pr is a ratio of velocity to temperature boundary layer thickness (if Pr=1, it means that velocity and thermal boundary layers grow together) formulated as:

$$\text{Pr} \approx \frac{\delta_u}{\delta_T} = \frac{\nu}{\alpha_f} = \frac{\left(\frac{\mu}{\rho}\right)}{\left(\frac{k_f}{\rho c_p}\right)} = \frac{\mu \cdot c_p}{k_f} \tag{2.6}$$

where ν is kinematic viscosity and α_f is thermal diffusivity of the fluid. The other variables are density ρ, thermal conductivity k_f, dynamic viscosity μ and specific heat capacity c_p.

Grashof Number

This parameter describes the natural convection. The Grashof number (Gr) measures the ratio of buoyancy forces to viscous forces. The buoyancy force induces fluid motion (to move up due to density difference), while the viscosity force acts as a movement resistance to the fluid and Gr can be described by:

$$\text{Gr} = \frac{\rho^2 \cdot \beta \cdot g \cdot L_c^3 \cdot \Delta T}{\mu^2} = \frac{\beta \cdot g \cdot L_c^3 \cdot \Delta T}{\nu^2} \tag{2.7}$$

where $\beta = 1/T_\infty$ is the thermal expansion coefficient, g is the constant of gravitation, L_c is the characteristic length of the surface, and ΔT is the temperature difference between the fluid and solid surface.

Rayleigh Number

Another important magnitude is the Rayleigh number (Ra), which measures the intensity of natural convection. This number is the product of Grashof and Prandtl numbers described as:

$$\mathrm{Ra} = \mathrm{Gr} \cdot \mathrm{Pr} = \frac{\beta \cdot g \cdot L_c^3 \cdot \Delta T}{\nu^2} \cdot \mathrm{Pr} \tag{2.8}$$

where a higher Ra value implies higher natural convection effects.

Reynolds Number

In a forced convection case, the important parameter is Reynolds Number (Re), which determines whether a fluid is in a laminar or turbulent flow state. Re is determined by the ratio of inertia forces to viscous forces and formulated as:

$$\mathrm{Re} = \frac{u_\infty \cdot L_c}{\nu} \tag{2.9}$$

where u_∞ is velocity and ν is kinematic viscosity of the fluid. There is also a critical Reynolds Number at which the flow becomes turbulent. The value of $\mathrm{Re}_{\mathrm{crit}}$ is dependent on the solid geometry.

Nusselt Number

This dimensionless parameter is determined by the ratio of two heat fluxes: the convective heat flux in the moving medium and the conductive heat transfer in the stationary fluid. It means that the Nusselt number (Nu) compares convection heat transfer with conduction heat transfer at a solid surface. High Nusselt numbers for heat transfer indicate a substantial convective heat transfer at the surface [4]. The below equation shows a correlation between Nu and the convective heat transfer coefficient α:

$$\mathrm{Nu} = \frac{\alpha \cdot L_c}{k_f} \tag{2.10}$$

Also, there is a correlation between the other dimensionless parameters and the Nusselt number, which is useful to calculate the convective heat transfer coefficient, formulated as:

$$\mathrm{Nu} = c \cdot \mathrm{Re}^b \cdot \mathrm{Pr}^n \quad \overset{\text{using eq. 2.10}}{\Longrightarrow} \quad \alpha = \frac{k_f}{L_c} \cdot c \cdot \mathrm{Re}^b \cdot \mathrm{Pr}^n \tag{2.11}$$

where the constants c, b and n depend on the solid geometry and type of flow (internal or external and laminar or turbulent).

The fluid in question is air, and its properties vary depending on the temperature it experiences. When air comes into contact with a solid surface, its properties are evaluated based on what is known as the "film temperature", in order to calculate the dimensionless numbers correctly. T_{film} is calculated as the average temperature of air and solids.

$$T_{\mathrm{film}} = \frac{T_{\mathrm{air}} + T_{\mathrm{solid}}}{2} \tag{2.12}$$

Chapter 3

State of the art

3.1 Automotive Headlamp

Headlamps on vehicles play a crucial role in ensuring adequate illumination using various light functions while avoiding the glare of oncoming traffic. They also should contribute to making the car easily visible on the road [9]. Developing a headlamp involves considering various criteria, such as performance, styling characteristics, functionality, energy consumption and LED technologies (other design cases still have Xenon technologies). The performance and appearance of vehicles are also dependent on headlamps. Customers and competition in the market have demanded the latest lighting technology and new styling characteristics, bringing more challenging geometries and functions to the headlamps [2].

Automotive lighting technology has been developing for over a hundred years. Gas lights were used in the first vehicles, and electric lights were introduced in the 1920s, followed by the development of optical and projection systems. Halogen light sources were developed in the 1960s and replaced by gas discharge lights (xenon) in the 1990s due to their improved brightness and longevity [9]. In the 21st century, LEDs were introduced in headlamps, replacing classic bulbs, thus achieving a higher level of modernity in vehicles. This illumination revolution was triggered by the new driving functions, high luminous efficiency, and increased safety LEDs provide [9].

3.1.1 Skin: Housing and Cover lens

The housing of the headlamp serves multiple purposes, acting as a container for all headlamp components, such as cables and reflectors. It is also responsible for securing the vehicle's headlamp and protecting against external elements like humidity and heat. Typically made from thermoplastics, the housing plays a crucial role in ensuring the durability and functionality of the headlamp assembly. Producing headlamp housings uses injection molding techniques, such as injecting grainy/molten thermoplastic material into a mold cavity designed to shape the headlamp housing. The material is injected under high pressure, replicating the housing design's intricate details with high precision, efficiency, and cost-effectiveness.

Figure 3.1: Full LED headlamp [10]

Cover lenses play an essential role in shaping the light distribution of automotive headlamps. Those

equipped with dispersion optics, as observed in the first image of Figure 3.2, manipulate the luminous flux, directing it to produce specific light distributions, such as cut-off lines [10]. However, the traditional patterned cover lens concept is being supplanted by non-patterned systems. The second image of Figure 3.2 shows a headlamp lens without dispersion optics, called clear cover lenses, which serve primarily as protective barriers against environmental factors like soiling and weather [10]. They find application in various headlamp systems, including inner lenses for low beam and high beam.

Figure 3.2: Headlamp cover lens with and without dispersion optics [10]

The selection of materials for headlamp lenses and housing, along with the overall design of the headlamp, plays a crucial role in determining its thermal behavior and susceptibility to fogging. Materials with high thermal conductivity facilitate efficient heat dissipation to the external environment, and those with low water vapor permeability are less prone to fogging. Additionally, the headlamp's shape and design, including the lens's curvature, can influence the extent of thermal radiation absorption from the sun. These material and design considerations introduce additional factors when devising effective cooling solutions for headlamp systems. Traditionally, cover lenses were crafted from glass, requiring impeccable quality to ensure transparency. However, the growing preference for plastic (Polycarbonate, PC) cover lenses offers significant advantages like impact resistance, lightweight properties, and greater design flexibility [10].

3.1.2 Light Module

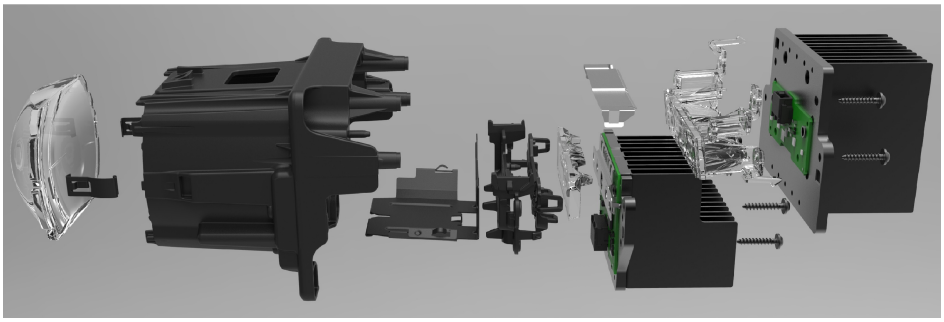

Figure 3.3: View of a light module [10]

An LED light module typically consists of multiple light-emitting diodes (LEDs) mounted on a printed circuit board (PCB) that is near a heat sink, as shown in Figure 3.3. In a printed circuit board (PCB) housing various LEDs, heat generation is critical due to the electrical energy converted into light. LEDs produce heat primarily through electron-hole recombination within their semiconductor materials. The heat generated varies depending on LED efficiency, operating current, and environmental conditions. Additionally, different types of LEDs may have varying thermal characteristics, such as maximum operating temperature. High-power LEDs typically generate more heat compared to lower-power variants. As the LEDs operate, heat accumulates within the PCB, potentially leading to temperature increases

that can affect performance and reliability. Therefore, effective thermal management strategies, such as heat sinks, thermal pads, and proper PCB layout design, are essential to dissipate heat and maintain optimal operating temperatures for the LEDs and the overall system, necessitating effective thermal management strategies to ensure optimal performance and longevity of LED systems.

LED

LED stands for "Light-emitting diode" and is a light source that converts electrical energy into light. They are produced in several designs, colors, and sizes, depending on the requirements [10]. LEDs offer high energy efficiency and design flexibility compared to previous lighting technologies, but these components tend to react very sensitively to heat and elevated temperatures [10].

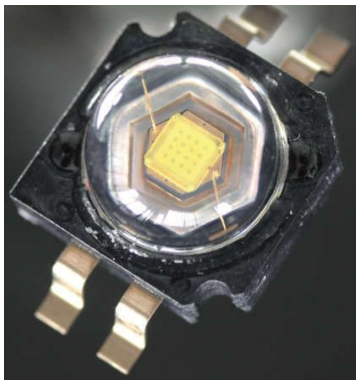

Figure 3.4: High Power LED [10]

In LEDs, the flow of electricity through the semiconductor material encounters resistance, resulting in heat generation. This phenomenon occurs through two primary mechanisms: "Joule-Effect" and "Photon Conversion". The Joule effect arises as electrons move through the semiconductor material, colliding with atoms, converting kinetic energy into thermal energy and elevating the temperature. Simultaneously, during LED operation, electrical energy is partly converted into light energy through photon emission. However, not all electrical energy is transformed into light, leading to some energy being lost as heat. Both processes contribute to the overall thermal load of the LED and surrounding components.

There are several reasons for managing the temperature of the headlamp and LED module. The effects are seen in the light output, color shift, and lifetime. When the operating temperature increases, the luminous efficiency decreases while the color of the light shifts with temperature change [1]. Therefore, the thermal design of an LED system is becoming critical as LEDs become more powerful and have a longer lifetime.

PCB

A printed circuit board (PCB) is a flat board composed of polymers and glass-epoxy materials, serving as a platform for mounting various electronic components like ICs, diodes, transistors, resistors, and capacitors to perform specific tasks. PCB also serves as a platform for mounting and arranging LEDs in a specific configuration, as shown in Figure 3.5, optimizing light distribution and efficiency.
In the PCB, heat is generated by the LEDs and other components such as resistors, transistors, and integrated circuits, each producing heat through similar electrical resistance and energy conversion mechanisms. Thermal vias are employed within the PCB structure to manage this heat effectively. Thermal vias are small holes drilled into the PCB, typically filled with a thermally conductive material like copper. These vias serve as pathways for heat to travel from the heat-generating components to the outer layers of the PCB, where it can be dissipated into the surrounding environment. Heat can be efficiently

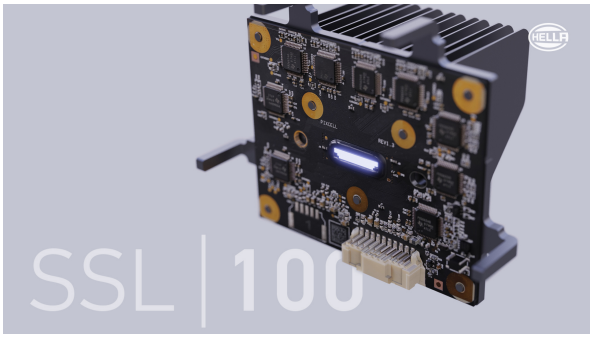

Figure 3.5: LEDs in a PCB contiguous to a heat sink in SSL 100 [10]

distributed and dissipated by strategically placing thermal vias near heat sources, such as LEDs, and connecting them to larger copper planes or heat sinks on the PCB's surface.

PCBs are typically cooled by direct contact with a fluid, i.e., air. However, when the boards are badly situated, an alternative cooling method involves using a cold plate, essentially a heat sink, as shown in Figure 3.5.

Heat Sink

Heat sinks are usually required in electronic devices to dissipate heat energy to the passing medium, in this case, the air. For the light module, a heat sink serves as a thermal management solution to dissipate the heat generated by the LEDs and PCB during operation, which helps maintain the temperature of the LEDs within the specified range. By incorporating fins on the base plate of the heat sink, the heat-transferring surface area can be increased. The increased surface area facilitates better convective cooling, improving thermal performance and preventing electronic components from reaching excessively high temperatures during operation [11].

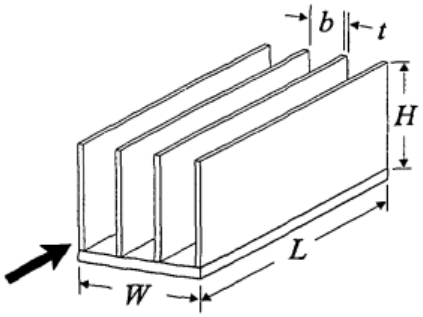

Dimensions	Symbol
Length of base plate	L
Width of base plate	W
Height of fin	H
Thickness of base plate	d
Space between fins	b
Thickness of fin	t
Number of fins	N

Figure 3.6: Plate fin heat sink geometry [11]

The geometry of the heat sink, illustrated in Figure 3.6, is required to calculate the heat transfer coefficient and the pressure drop (influence on volume flow rate). It can be a challenge because of several configurations (geometry, material and surface) offered by the manufacturer. The selection process includes performance, dimensional measurements, available airflow and cost.

3.1.3 Fan

Natural convection is the preferred way to cool electronic systems for many reasons, such as cost, noise and simplicity, which the forced convection can not offer. However, natural convection is often insufficient to extract all the energy from the light module. Therefore, fans are required to ensure an appropriate cooling of the LED module.

Fans belong to the field of turbo-machinery as a powered machine. They absorb energy to increase the fluid pressure, creating airflow. A fan contains a motor, housing, rotating assembly of blades, and a hub, known as an impeller. There are three types of fans, as shown in figure 3.7, axial-, radial- and diagonal fans. The difference relies on the direction of the central air stream and pressure characteristics. In axial fans, the airflow direction is parallel to the rotation axis of the impeller. They can deliver a high flow rate but are suitable for systems with low pressure. On the other hand, the radial or centrifugal fans deliver low flow rates to systems but against high pressure. Lastly, there are diagonal and mixed flow fans from axial- and radial fans.

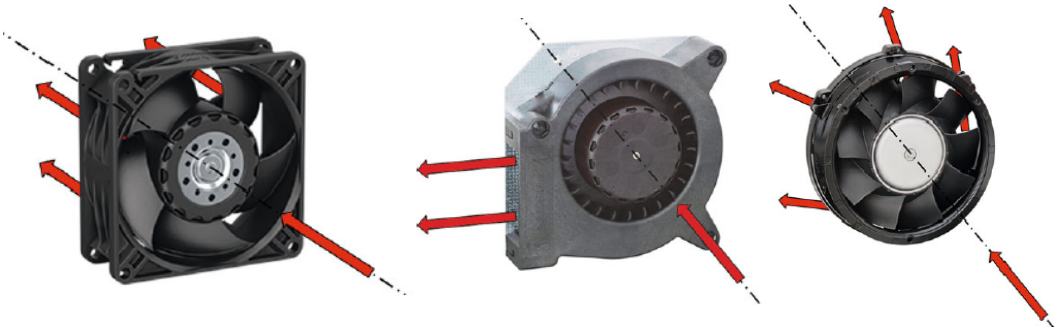

Figure 3.7: Types of fan: axial, radial and diagonal fan [12]

Fan performance is exhibited in the characteristic curve, which fan manufacturers provide to help engineers with the selection of fans. The fan characteristic curve shows the relationship between the volumetric flow rate and the pressure drop of a fan. A fan delivers its maximum volume flow when it is freely positioned. If installed in a device, the airflow must overcome the system's flow resistance, which is determined by the system's static pressure head. The airflow rate is determined by the operation point of the fan, as shown in Figure 3.8, which is the intersection between the fan characteristic curve and the system curve.

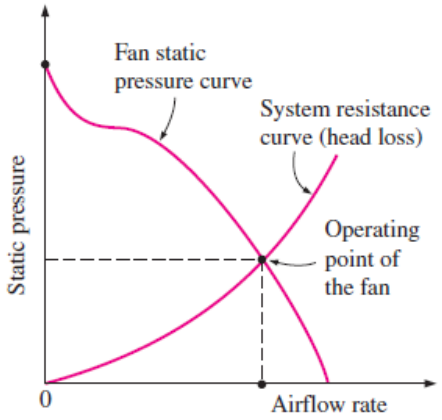

Figure 3.8: Characteristic curve of a fan [5]

Airflow design within the headlamp assembly is essential for managing temperature. Well-designed systems incorporate strategically positioned air guides and channels that facilitate the air exchange within the headlamp. This airflow is achieved through natural convection and, in some cases, aided by fans. Therefore, the position of the fans inside the headlamp plays a crucial role in cooling, influencing the airflow. Some configurations may include placing the fan below the heat sink or between two heat sinks adjacent to an air guide that will be divided for different heat sinks or directly to PCBs.

3.2 Computational Fluid Dynamics

Computational Fluid Dynamics (CFD) is essential across engineering fields for several reasons. Firstly, it aids in design optimization by allowing engineers to explore and improve designs quickly and affordably. By simulating fluid flow and heat transfer in different scenarios, CFD can identify potential design issues and enhance performance before physical prototypes are built, saving time and money. CFD simulations help optimize the thermal system and predict the defogging behavior inside the headlamp. Finally, CFD reduces costs by replacing the need for physical prototypes and experimental tests with virtual evaluations, resulting in more cost-effective engineering solutions [13].

CFD is a branch of fluid mechanics that employs numerical methods and algorithms to solve and analyze fluid flow problems. The theoretical background of CFD involves several key concepts and principles:

Navier-Stokes Equations: The Navier-Stokes equations constitute a set of nonlinear differential equations that serve as a fundamental framework for expressing the principles of mass, momentum, and energy conservation within a system [13]. The foundation of contemporary CFD programs is rooted in these equations.

Boundary conditions: They are crucial for defining how fluid behaves at the boundaries of a computational domain according to the Navier-Stokes equations. They specify interactions with solid walls, inlets, and outlets, ensuring the model accurately reflects physical flow. For example, fluid velocity is zero at a no-slip wall, simulating surface adhesion. Inlet conditions define fluid entry, while outlets allow smooth exit, which is vital for accurate computational fluid dynamics simulations. Often based on measurements or known principles, these conditions offer valuable insights into real-world fluid dynamics. [13]

Discretization: Discretization involves dividing the continuous fluid flow domain into discrete elements or cells, enabling numerical methods to approximate solutions [13]. Since the Navier-Stokes equations are continuous, they must be discretized to be solved numerically on a computer. Discretization methods are finite difference, finite volume and finite element methods.

At Hella GmbH, the current headlamp testing procedures involve using CFD simulations. These simulations aim to optimize thermal systems, enhancing cooling mechanisms and airflow to minimize thermal issues. Initially, these CFD simulations were developed and validated through experimental tests conducted in climate chambers and via thermography. Figure 3.12 shows a representation of the climate chamber with a headlamp inside in 3D design available for the CFD simulation. This robust validation process serves as the foundation for the methodology applied in this work. The next step involves applying a similar approach to validate the Modelica modeling using diverse boundary conditions as input parameters. Subsequently, the results of the Modelica simulations will be compared with those of the previously conducted CFD simulations in the same headlamp across various test cases. It is important to note that these test cases were initially replicated within climate chambers. Understanding this relationship between CFD simulations and the processes occurring within climate chambers is vital; therefore, it will be explained in the next section. Ultimately, the goal is for the Modelica model to faithfully represent the results obtained from the CFD simulations.

3.3 Thermal and Climate Tests: Climate Chamber

A climate chamber, also known as an environmental chamber or temperature chamber, is a controlled environment used for testing the behavior of materials, components, or products under various temperature, humidity, and sometimes pressure conditions. These chambers simulate real-world environments to assess how the tested items perform and withstand different climatic conditions.

The general concept of a climate chamber involves creating a chamber with precise control over temperature, humidity, and airflow. This control allows researchers, engineers, and manufacturers to subject their products to extreme conditions or specific environmental parameters to evaluate their performance, durability, and reliability. Climate chambers play a vital role in product development, quality control, and research, helping companies ensure their products meet regulatory standards, withstand harsh environmental conditions, and perform reliably in real-world scenarios.

3.3.1 Single Climate Chamber (SCC)

Single-area climate chambers typically have a well-insulated enclosure with adjustable walls, floors, and ceilings to accommodate different test setups. Heating and cooling systems, humidity generators, air circulation fans, and sensors are integrated into the chamber to maintain the desired environmental conditions. In the first image of Figure 3.9, a 3D rendering displays a headlamp positioned on a base. Notably, an inlet (yellow) is visible, serving as a control point for regulating the temperature and humidity of the incoming air. Moving to the second image, airflow patterns are depicted at ambient temperature as the air inlet is deactivated, resulting in the assumption that natural convection prevails around the headlamp, characterized by minimal air velocities.

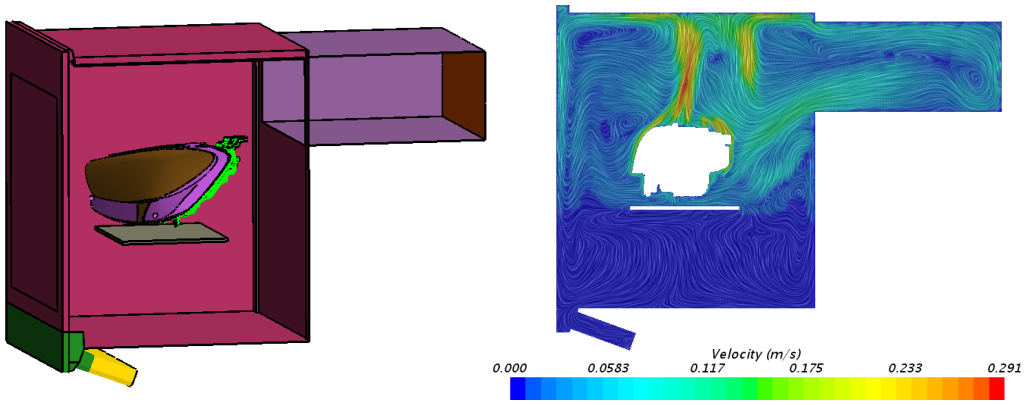

Figure 3.9: View of a headlamp and its streamline simulation at ambient temperature in SCC [14]

3.3.2 Double Climate Chamber (DCC)

The Double Climate Chamber consists of front and rear sections. Each fulfills specific functions. The DCC model at Hella GmbH is based on the double-area chamber the vendor "Vötsch" created. It can have a wind fan, rain shower, and vacuum unit [15]. Additionally, the system can be expanded to include a sun simulation, creating a comprehensive package that fulfills all testing requirements.

Figure 3.10: Double climate chamber from Vötschtechnik [15]

The company Vötsch provided a detailed 3D CAD model that was simplified for simulations. Figure 3.11 overviews the entire climate chamber geometry and its components. These areas are separated by a flexible separator wall, which can act as either a baffle for isolation or an internal interface for connection purposes. Air circulation is facilitated through front and rear inlets, while outlets on both sides enable the expulsion of air. However, this setup simplifies the lives of the fans behind these outlets. Additionally, optional features like the blower and air guide baffle cater to specific scenarios like driving and defogging load cases. Finally, the fixing plate, positioned below the opto-mechatronic device, prevents unwanted cooling effects from the inlet air. This comprehensive representation ensures that the model accurately reflects real-world conditions and allows versatile simulation scenarios.

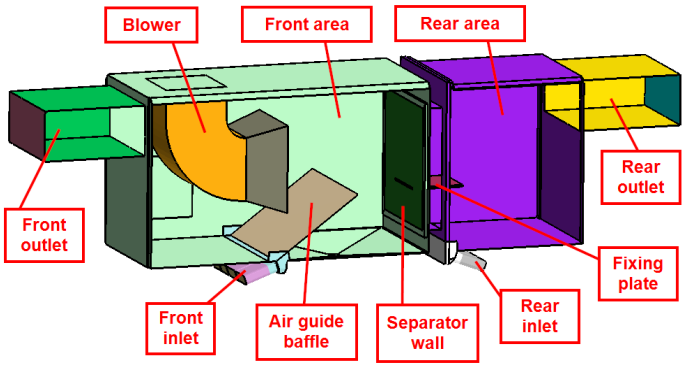

Figure 3.11: Parts of the DCC [14]

3.3.3 Simulation Cases

In the simulation model, the choice between SCC and DCC depends on the specific requirements of each test case.

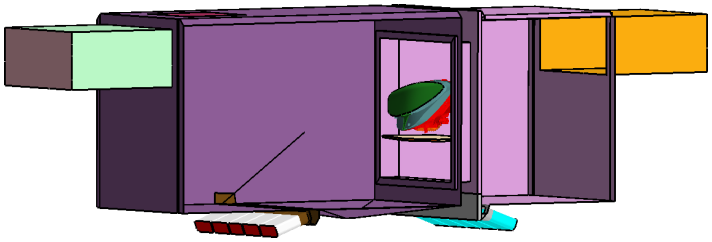

Figure 3.12: 3D DCC representation for one temperature [14]

Approval tests for headlamps are evaluations conducted to ensure that headlamp designs comply with regulatory standards and meet safety requirements before being approved for vehicle use. Both SCC and DCC models are applicable for the "Type-Approval" test conducted at 22–25 °C as ambient temperature across the entire headlamp. When the engine is turned off, one temperature for the whole headlamp does not influence the temperature. However, tests at higher ambient temperatures, such as 35 °C, 45 °C or 75 °C, for the entire headlamp are usually required by the customer; in that case, only one climate area (SCC) must be computed to accurately represent the test conditions. Figure 3.12 shows the setup for the "Type-Approval" test in a double climate chamber, with no separator wall because only one temperature is required. In this working mode, as the ambient temperature is needed, all baffles and air inlets are disabled. The boundary conditions are adjusted according to the specific use-case requirements. In the CFD simulation, shown in Figure 3.13, the airflow is observed at low velocities as the air front and rear inlets are deactivated. Additionally, it is evident that there is no separation between the areas, as there is continuous airflow across the regions. In this test at ambient temperature, the heat

transfer between the outside and headlamp can be categorized as natural convection, as there is no fan or extra air inflow.

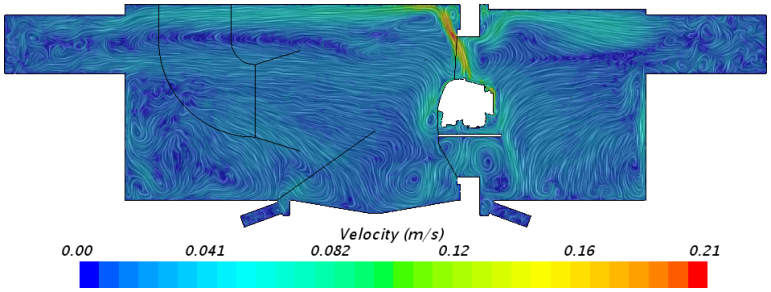

Figure 3.13: Streamline at ambient temperature ("Type-Approval" test) in DCC [14]

Other test cases include a temperature adjustment at the rear, representing the engine as a heat source. It comes into play when the automobile is turned on or running. The engine's heat, combined with other factors, can elevate the temperature inside the headlamp, precisely changing the ambient temperature near the headlamp due to its proximity to the housing covered by the chassis. To simulate the thermal behavior in that case, the engine's heat needs to be considered, called the "High-Temperature" test, at two different temperatures, one for the housing surface called rear temperature and another for the cover lens area, which is the outside ambient temperature called front temperature. DCC may be required due to its capability to handle multiple climate areas. Similarly, driving and defogging use cases must be simulated using DCC, as they involve dynamic elements such as wind representation with blowers and activation of air guide baffles and inflows in the climate areas, which DCC accommodates effectively.

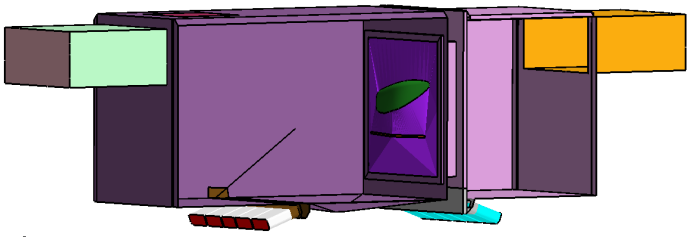

Figure 3.14: 3D DCC representation for two different temperatures [14]

In order to get high temperatures in the climate chamber, the air inflows and boundary conditions are adjusted according to the specific requirements of the use-case scenario. The setup can be seen in Figure 3.14 and the air velocities in Figure 3.15, where a separation between the two areas is visible because of the necessity of two temperatures T_{front} and T_{rear} (there is no air mixing between the two areas). The air inlets enable precise control over the airflow within the system, ensuring that air is directed effectively to meet the specific requirements of the intended application.

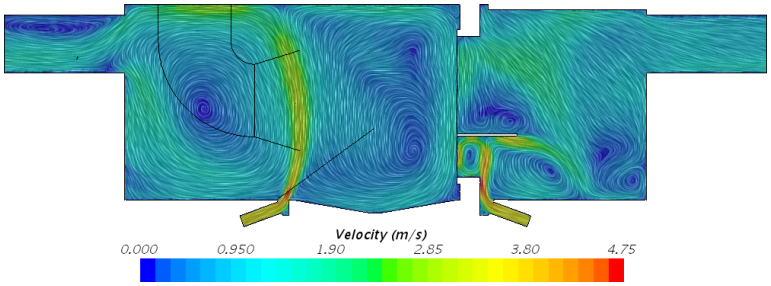

Figure 3.15: Streamline at two different temperatures ("High-Temperature" test) in DCC [14]

Chapter 4

Development of the Modeling

In this chapter, the modeling development will be discussed, starting with the basic components available in the Modelica Library and ending with their integration into an equation-based model representing different elements (heat sink, housing, and cover lens) as an overall model of the headlamp. Different mathematical approaches will also be covered and implemented into the components in order to calculate essential parameters such as the heat transfer coefficient and volume flow.

4.1 Object-Oriented Modeling of Physical Systems: Modelica

Object-oriented modeling is an increasingly prominent field within modeling and simulation, providing a systematic approach to mathematical and equation-based modeling [16]. Modelica was created to model and simulate complex physical systems, e.g., mechanical, electrical, electronic, magnetic, hydraulic or thermal systems, following mathematical equations and achieving a simulation based on the fundamental principles. To solve problems with the Modelica language, a modeling and simulation environment is required to define a model with a Graphical User Interface (GUI) to efficiently simulate the modeling with standard numerical integration methods and visualize the results [17]. To meet that necessity, an open-source simulation environment called OpenModelica was developed by Linköping University in collaboration with the Open Source Modelica Consortium (OSMC). An important aspect of this work is to do the entire modeling with the programming language Modelica using OpenModelica.

4.2 Modelica Components

The entire model of the thermal headlamp system forms a thermo-fluid network consisting of conductive and convective heat transfer. These components, see Figure 4.1, were sourced from the Thermal Library of Modelica [18] and subsequently adapted, preserving their fundamental equations. This library enables the modeling of a 1D thermal system. It offers heat transfer components and a simple thermo-fluid pipe flow. The coupling of the respective models is achieved via "HeatPorts" (thermal connectors) and "FluidPorts" (flow connectors) [19]. The potential variable for both connectors is the temperature (T). In Figure 4.1, the connectors for heat flow have a square shape, while flow connectors have an arrow shape (based on the ThermoFluidStream Library from DLR [20]).

Thermal Resistor

Developing an analogy with electrical concepts to find an interesting application in thermal engineering, it is noticed that heat transfer is analogous to a current and temperature difference is analogous to a

potential difference [7]. This relationship is formulated as follows:

$$\dot{Q} = \frac{\Delta T}{R_{\text{th}}} = G \cdot \Delta T \tag{4.1}$$

where R_{th} is thermal resistance and ΔT is the temperature difference. The equation can also be formulated with a thermal conductance G (= inverse of thermal resistance). This thermal resistor component represents the thermal resistance of the wall against heat conduction and is formulated as:

$$R_{\text{th,cond}} = \frac{d}{k \cdot A} \tag{4.2}$$

where d is the thickness of the wall (housing or cover lens), k is the material's thermal conductivity and A is the effective area for conduction.

Convection

This component represents linear heat convection of the surface and the fluid. The heat flow passing from the solid to the air (or inverse) is proportional to the temperature difference, given as:

$$\dot{Q}_{\text{solid}\rightarrow\text{air}} = \alpha \cdot A_{\text{solid}} \cdot (T_{\text{solid}} - T_{\text{solid}}) \tag{4.3}$$

where A_{solid} is the effective area for convection and α is the heat transfer coefficient. This equation can also be given with a thermal resistance based on the equation (4.1), and it is formulated as:

$$R_{\text{th,conv}} = \frac{1}{\alpha \cdot A} \tag{4.4}$$

Heat Capacitor

To run a dynamic simulation, the heat capacity C_{th} of the system must be considered. The heat capacity depends on the specific heat capacity c_p and the mass m of an object, see equation (4.5). Additionally, the heat capacity C_{th} can also be described with the change in temperature T and the heat transfer rate $\dot{Q}$.

$$C_{\text{th}} = c_p \cdot m = \frac{\dot{Q}}{\dot{T}} \tag{4.5}$$

Airflow

This component represents the heating or cooling of the internal air through convection. Heating occurs when the air takes the thermal power from the heat sink at the walls of the flow channels, while cooling occurs when the internal air drives the heat out through the housing. The energy balance applies:

$$\dot{Q}_{\text{solid}\rightarrow\text{air}} = \dot{Q}_{\text{inlet}\rightarrow\text{outlet}} \tag{4.6}$$

As the air receives the heat from the heat sink, its temperature increases. When the air is in contact with the cool surface of the housing, the air temperature cools. After the heat transfer process, the final temperature (T_{out}) is determined by:

$$\dot{Q}_{\text{in}\rightarrow\text{out}} = \dot{m} \cdot c_p \cdot \Delta T = \dot{V} \cdot \rho \cdot c_p \cdot (T_{\text{out}} - T_{\text{in}}) \tag{4.7}$$

The equation (4.7) was obtained by an energy balance equation (4.8). This equation states that the sum of the air enthalpy flow rates of heat transfer at the inlet ($\dot{H}_{\text{in}}$) and outlet ($\dot{H}_{\text{out}}$) of a system, along with

any heat generation or absorption ($\dot{Q}$), must equal zero, ensuring that energy is conserved within the system.

$$\dot{H}_{\text{in}} + \dot{Q} + \dot{H}_{\text{out}} = 0 \tag{4.8}$$

The enthalpy flow rates and the temperature are formulated as:

$$\dot{H} = \dot{m} \cdot h \quad \text{and} \quad T = \frac{h}{c_p} \tag{4.9}$$

where h is the specific enthalpy and c_p is the specific heat capacity of the air. The mass flow $\dot{m}$ and volume flow $\dot{V}$ are parameters given by the fan.

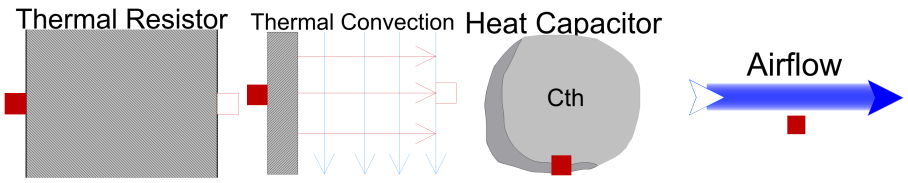

Figure 4.1: Visualization of the basic components in Modelica [18]

4.3 Theoretical Analysis: Parameters

This section will explain all the analytical and mathematical approaches applied in the modeling, developing an understanding of all the headlamp's components, such as the heat sink, fan, housing and cover lens, and their respective parameters. The following equations will be implemented in the existing basic components or in the integrated partial components of the new library (developed by this work) in Modelica.

4.3.1 Heat Transfer at Housing and Cover lens

Figure 4.2 illustrates the relevant variables and inputs for describing the heat transfer across the headlamp's shell from the internal air to the ambient. This heat transfer is represented by two convective thermal resistances and one conductive thermal resistance, following the equations (4.2) and (4.4).

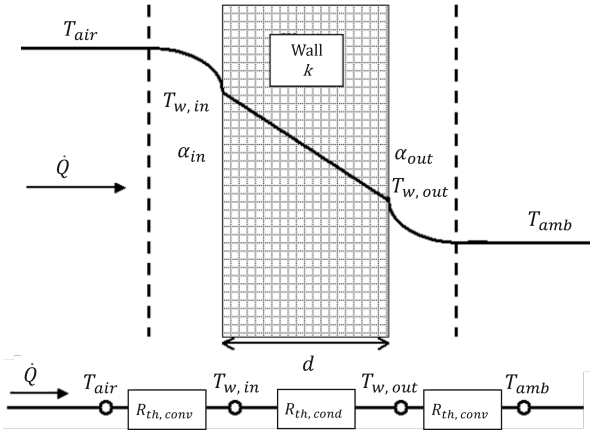

Figure 4.2: Schematic of the heat transfer at the housing and cover lens

The total thermal resistance of the housing/cover lens is given by:

$$\text{R}_{\text{th,total}} = \text{R}_{\text{th,conv,in}} + \text{R}_{\text{th,cond}} + \text{R}_{\text{th,conv,out}} = \frac{1}{\alpha_{\text{in}} \cdot A} + \frac{d}{k \cdot A} + \frac{1}{\alpha_{\text{out}} \cdot A} \tag{4.10}$$

where α_{in} and α_{out} are the convective heat transfer coefficients, d is the thickness of the cover lens and housing, k is the thermal conductivity of the material and A is the effective area for the heat transfer.

The heat flow $\dot{Q}$ between the two points with temperatures $T_{\text{wall,in}}$ and $T_{\text{wall,out}}$ will be given as input. The ambient temperature T_{ambient} is given by the CFD simulation based on the climate chamber according to the requirements of each test case. Important variables like cross-sectional area A with thickness d and thermal conductivity k of the housing are also known from the beginning. The most important parameter to calculate $T_{\text{wall,out}}$ and then T_{air} is the heat transfer coefficient. Therefore, the following approaches (based on Nu correlation depending on the different flow characteristics) are applied in the modeling to calculate α_{in} and α_{out}. All the following equations were obtained from VDI Heat Atlas [21].

Natural Convection at Housing and Cover lens

This approach will be used at ambient temperature (25℃) for the "Type-Approval" test, as shown in Figure 3.13, where there is no blower or fan outside the headlamp. For vertical plates, where the characteristic length (L_c) is the height of the cover lens or housing, the Nusselt number is formulated as:

$$\text{Nu} = \left[0.825 + 0.387\,(\text{Ra} \cdot f_1(\text{Pr}))^{1/6}\right]^2 \tag{4.11}$$

where Pr and Ra are formulated in the equations (2.6) and (2.8), and $f_1(\text{Pr})$ is determined by:

$$f_1(\text{Pr}) = \left[1 + \left(\frac{0.492}{\text{Pr}}\right)^{9/16}\right]^{-16/9} \tag{4.12}$$

For horizontal plates with the characteristic length given as: $L_c = \frac{A}{P}$, there are two cases. The first one is for upper surfaces, where the Nusselt number is defined as:

$$\text{Nu} = 0.766 \cdot [\text{Ra} \cdot f_2(\text{Pr})]^{1/5} \quad \text{for laminar flow Ra} \cdot f_2(\text{Pr}) \leq 7 \times 10^4 \tag{4.13}$$

and

$$\text{Nu} = 0.15 \cdot [\text{Ra} \cdot f_2(\text{Pr})]^{1/3} \quad \text{for turbulent flow Ra} \cdot f_2(\text{Pr}) > 7 \times 10^4 \tag{4.14}$$

where $f_2(\text{Pr})$ is given by:

$$f_2(\text{Pr}) = \left[1 + \left(\frac{0.322}{\text{Pr}}\right)^{11/20}\right]^{-20/11} \tag{4.15}$$

The second case is for lower surfaces, where the Nusselt number is defined as:

$$\text{Nu} = 0.6 \cdot [\text{Ra} \cdot f_1(\text{Pr})]^{1/5} \quad \text{for } 10^3 < \text{Ra} \cdot f_1(\text{Pr}) < 10^{10} \tag{4.16}$$

Forced Convection at Housing and Cover lens

In order to manage two temperatures in the climate chamber, there are two air inflows impulsed by an external force (blowers), increasing the heat transfer coefficient compared to natural convection due to a higher velocity, as observed in Figure 3.15. The cover lens and housing can be considered as vertical and horizontal surfaces. Therefore, Reynolds number (Re) is given as:

$$\text{Re} = \frac{u_\infty \cdot L_c}{\nu} \tag{4.17}$$

where u_∞ is the velocity of the air and ν is kinematic viscosity of air. Considering the cover lens as a plate, the characteristic length L_c is the length or height of the plate. Depending on the flow condition, the Nusselt number is formulated as:

$$\text{Nu} = 0.664 \cdot \text{Re}^{0.5} \cdot \text{Pr}^{1/3} \quad \text{for laminar flow} \tag{4.18}$$

and

$$\text{Nu} = \frac{0.037 \cdot \text{Re}^{0.8} \cdot \text{Pr}}{1 + 2.443 \cdot \text{Re}^{-0.1} \cdot (\text{Pr}^{2/3} - 1)} \quad \text{for turbulent flow} \tag{4.19}$$

Modelica Representation

In Modelica, the components called "Housing" and "Coverlens" were created by integrating the basic components having the same structure, as shown in Figure 4.3, but they differ from the required parameters to describe the inner and outer convection. Two components for convection and one for conduction are implemented to model the heat transfer at the housing/cover lens. The geometry data, like thickness k and area A, will calculate the thermal resistance, representing the thermal conduction for both components. The component that represents the airflow is also included. The airflow takes the heat out of the heat sink and releases it into the environment through the housing and cover lens. This means that after the heat transfer with the ambient, the temperature at the outlet will be lower than the inlet temperature, calculated by the equations (4.6) and (4.7).

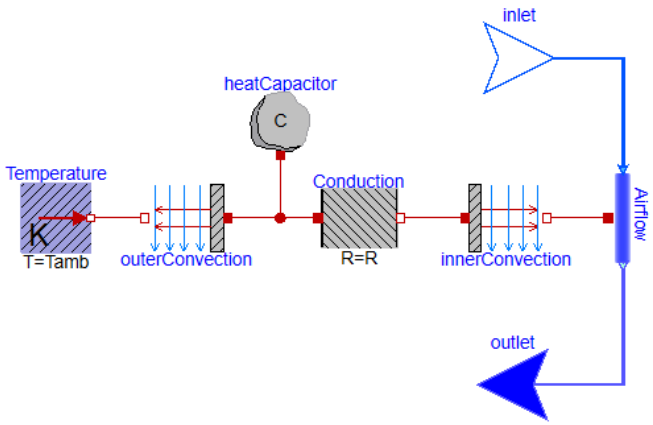

Figure 4.3: Modelica representation of the housing and cover lens [18]

Regarding the component "Coverlens", the Nusselt correlation can help determine the heat transfer coefficients using natural or forced convection approaches. The cover lens tends to be a vertical wall, so it can easily be adapted in 1D modeling. The equation (4.19) will be applied in the presence of a fan, and the equation (4.11) for natural convection. Applying these equations, it is observed that an average velocity is required and will be provided as an input (also explained in Section 5.2). After the Nusselt number is calculated with the correct approach, the heat transfer coefficient is then given by:

$$\alpha = \frac{\text{Nu} \cdot k_f}{L_c} \tag{4.20}$$

where k_f is the thermal conductivity of the fluid and L_c is the characteristic length.

While for the component "Housing", because of the complex geometry of the housing and black cover lens in 1D modeling (horizontal and vertical plates) and the lack of information to calculate the velocities near the housing, the Nusselt correlation is not suitable here. Therefore, heat transfer coefficients are provided as inputs.

4.3.2 Heat transfer at Light Module

When the PCB is exposed to the air without a heat sink, the convective heat transfer is dominant, and the heat transfer coefficient can be calculated using the equations for a Re and Nu correlation. On the other hand, when the thermal power of the LED is too high, a heat sink is required and placed next to a PCB, enhancing thermal conduction. Therefore, two heat transfer mechanisms need to be described: conduction from the LED to the fins of the heat sink through the PCB and convection from the heat sink to air, as shown in Figure 4.4.

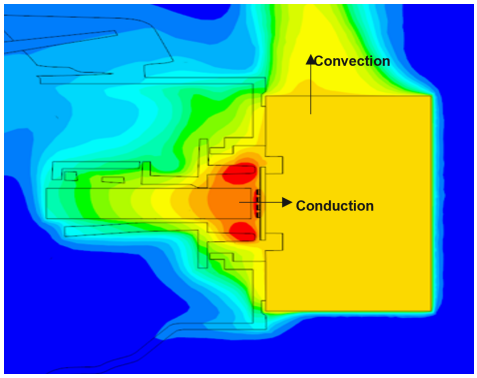

Figure 4.4: Heat transfer mechanisms at the light module [14]

Thermal Resistance of LED module

The thermal behavior of an LED module can be described with the total thermal resistance R_{th}, which is the sum of the thermal resistances of each component (LED, PCB and heat sink base plate). The PCB establishes the connection between the LEDs and the heat sink, constructed from different layers with different thermal properties, as shown in Figure 4.5. To calculate the LED temperature, the heat flow $\dot{Q}$ of the system must be known because a temperature gradient arises from junction to ambient, i.e., the chip temperature T_{junction} of the LED increases until the system achieves thermodynamic equilibrium [3]. The maximum temperature rise is therefore given by [3]:

$$\Delta T = P_{\text{th}} \cdot R_{\text{th}} \tag{4.21}$$

where P_{th} is the thermal power loss and R_{th} the LED thermal resistance.

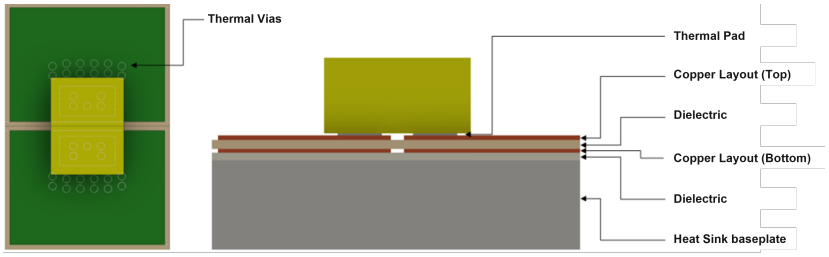

Figure 4.5: Schematic of the PCB [22]

The heat flux is introduced into the PCB through the thermal pads. Since the area of the pads is relatively small, the first copper layer is intended to ensure good heat spreading so that the heat is distributed over a large area as much as possible. The upper dielectric layer underneath separates the two copper layers and has low thermal conductivity. In order to enhance thermal conduction, the copper layers are interconnected by copper-filled thermal vias, also known as through-holes [22]. These vias can be arranged both directly under the thermal pads and above/below the LEDs, as shown in Figure 4.5. The

lower dielectric layer has a higher thermal conductivity and provides the connection to the heat sink base plate. Table 4.1 shows the thermal conductivity values depending on the material.

Material	Thermal Conductivity
Copper (Cu)	398 W/mK
Dielectric 1 (FR4)	0.37 W/mK
Dielectric 2	1.3 W/mK

Table 4.1: Common components in a PCB

The thermal resistance of each component will be calculated using the equation (4.2). This approach assumes a uniform heat flux density over the entire area of the heat sink base plate. However, in reality, the heat is not evenly dispersed, considering the heat spreading from the hot spots (where the LEDs are located). With analytical approaches, Heat spreading is a complex phenomenon that can be addressed accurately in geometrically simple cases. However, when multiple sources or layers (such as in PCB) are involved, the problem becomes intractable from an approximate analytical point of view [23]. In contact with the heat sink, the conductive heat transfer through the base plate is formulated as follows:

$$\dot{Q} = \frac{k}{d} \cdot A_{\text{bp}} \cdot \Delta T \tag{4.22}$$

where k is the thermal conductivity of the material and d is the thickness of the base plate. A_{bp} (= $L \cdot W$) is the area of the heat sink base plate, see Figure 3.6 to find L and W.

Convective Heat Transfer Coefficient at Heat Sink

In order to calculate the temperatures of the air and heat sink, the equation (4.3) can be formulated as:

$$\dot{Q}_{\text{hs}\rightarrow\text{air}} = \alpha \cdot A_{\text{hs}} \cdot (T_{\text{hs}} - T_{\text{air}}) \tag{4.23}$$

where A_{hs} is the total heat sink surface involved in the convective heat transfer and can be calculated with the heat sink geometrical parameters from Figure 3.6 given as:

$$A_{\text{hs}} = (L \cdot W) + (2 \cdot H \cdot (L + t) \cdot N) \tag{4.24}$$

Knowing the heat transfer coefficient is essential for assessing the effectiveness of heat dissipation because it determines how efficiently heat is transferred from the heat sink into the surrounding environment, i.e., the internal air in the headlamp. An analytical approach has been developed by Teertstra et al. [11] to predict the average heat transfer coefficient for forced convection-cooled plate-fin heat sinks. The heat transfer coefficient depends on various factors, including the geometry and material properties of the heat sink involved and the surrounding fluid (air). By knowing the heat transfer coefficient, a better and optimized heat sink design can be developed to ensure that the PCB operates within safe temperature limits, thus improving its reliability and performance.

The ideal values would be when the fin efficiency is 1, i.e. T_{fin} is equal to the temperature at the base plate $T_{\text{baseplate}}$. For this case, the ideal Nusselt number $\text{Nu}_{\text{hs,ideal}}$ is determined by:

$$\text{Nu}_{\text{hs,ideal}} = \left[\left(\frac{1}{0.5 \cdot \text{Re}_{\text{b}} \cdot \text{Pr}} \right)^3 + \left(\frac{1}{0.664 \cdot \sqrt{\text{Re}_{\text{b}}} \cdot \text{Pr}^{1/3} \cdot \sqrt{1 + 3.65 \left(\text{Re}_{\text{b}}^{-1/2} \right)}} \right)^3 \right]^{-1/3} \tag{4.25}$$

where

$$\text{Re}_b = \frac{(V_{\text{ch}} \cdot b)}{\nu} \cdot \frac{b}{L} \tag{4.26}$$

is the modified channel Reynolds number and

$$V_{ch} = \frac{\dot{V}}{A_{inlet}} = \frac{\dot{V}}{H \cdot b \cdot (N-1)} \tag{4.27}$$

is the average velocity in the channel. $\dot{V}$ is the volume flow rate given by the fan. For more accuracy, the fin efficiency has to be considered because of the temperature variations between the fins and the base plate, i.e. $T_{fin} < T_{baseplate}$

$$Nu_{hs} = \eta \cdot Nu_{hs,ideal} \tag{4.28}$$

The fin efficiency (η) can be also determined as:

$$\eta = \frac{\tanh\left(\sqrt{2Nu_{hs,ideal}\frac{k_f}{k}\frac{H}{b}\frac{H}{t}\left(\frac{t}{L}+1\right)}\right)}{\sqrt{2Nu_{hs,ideal}\frac{k_f}{k}\frac{H}{b}\frac{H}{t}\left(\frac{t}{L}+1\right)}} \tag{4.29}$$

Replacing equation (4.25) and (4.29) in the equation (4.28) gives the following equation:

$$Nu_{hs} = \frac{\tanh\left(\sqrt{2Nu_{hs,ideal}\frac{k_f}{k}\frac{H}{b}\frac{H}{t}\left(\frac{t}{L}+1\right)}\right)}{\sqrt{2Nu_{hs,ideal}\frac{k_f}{k}\frac{H}{b}\frac{H}{t}\left(\frac{t}{L}+1\right)}} \cdot Nu_{hs,ideal} \tag{4.30}$$

The average convective heat transfer coefficient is given as:

$$\alpha = \frac{Nu_{hs} \cdot k_f}{b} \tag{4.31}$$

Modelica Representation

This representation in Figure 4.6 includes a series of thermal resistances of each component until the convection heat transfer between the heat sink fins and the air. Each thermal resistor has three parameters: area A, thickness d and thermal conductivity k of the material. Thermal convection was implemented to describe the thermal behavior between the heat sink and air. The heat flow (given by the parameter $P_{th,\,LM}$ in Figure 4.6) and the convective area A_{hs} are known inputs used to calculate the temperature difference. However, the heat transfer coefficient needs to be calculated; therefore, the equations of Section 4.3.2 are implemented in this partial component called "Light module".

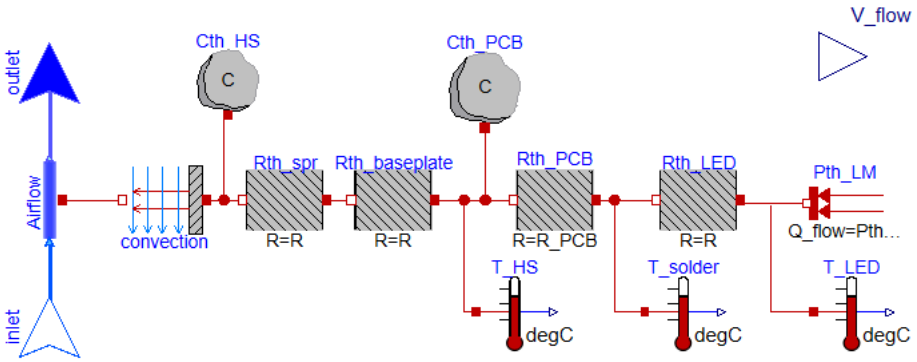

Figure 4.6: Modelica representation of the light module [18]

Evaluating the parameters, aside from geometrical parameters from Figure 3.6 (also implemented in this component), to calculate the heat transfer coefficient at the heat sink, from the equation (4.27), the

volume flow rate is a required parameter but unknown in the early development stages because it is dependent on the pressure drop, as observed in Figure 3.8. Therefore, a mathematical approach is applied to calculate the heat sink's pressure drop, which is derived as an output from the light-module component and used as input by the fan component, explained in the next section.

4.3.3 Volume Flow Rate of the Fan

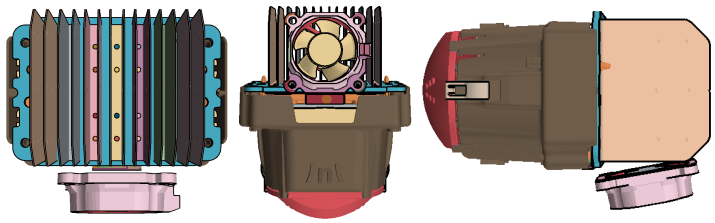

Figure 4.7: View of a light module with a fan under the heat sink [14]

The fan manufacturer typically provides the fan characteristic curve such as Figure 3.8. To simplify the calculation of the volume flow rate, an approximation of the fan curve can be expressed with an equation, which are often non-linear. This equation represents a correlation between the pressure drop and the volume flow rate of the air. The equation (4.32) was obtained from a plot digitizer and provides a reasonable estimate of the fan performance curve and was obtained from the fan used in the simulated headlamps. This equation will be implemented in the "Fan" component.

$$\begin{aligned}\Delta P_{\text{Fan}} =& 9.57 \cdot 10^{-5} \cdot \dot{V}_{\text{Fan}}^{6} - 5.06 \cdot 10^{-3} \cdot \dot{V}_{\text{Fan}}^{5} + 9.67 \cdot 10^{-2} \cdot \dot{V}_{\text{Fan}}^{4} \\ & - 0.81 \cdot \dot{V}_{\text{Fan}}^{3} + 3.09 \cdot \dot{V}_{\text{Fan}}^{2} - 12.33 \cdot \dot{V}_{\text{Fan}} + 87.06\end{aligned} \tag{4.32}$$

An integrated approach, developed by Culham and Muzychka [24], for incorporating forced convection through the specification of a fan curve is employed within the optimization procedure. This approach establishes a direct link between the optimized design parameters of the heat sink and the fan's operating point. The pressure drop experienced by the air flowing through the heat sink is formulated as follows:

$$\Delta P_{\text{hs}} = \left(K_c + f_{\text{app}} \left(\frac{N \cdot (2HL + bL)}{H \cdot W} \right) + K_e \right) \cdot \frac{\rho(V_{\text{ch}}^2)}{2} \tag{4.33}$$

The expansion and contraction loss coefficients are defined using the simple expressions for a sudden contraction and a sudden expansion:

$$K_c = 0.42 \cdot (1 - \sigma^2), \quad K_e = (1 - \sigma^2)^2 \tag{4.34}$$

where $\sigma = 1 - \frac{Nt}{W}$. The apparent friction factor for a rectangular channel may be computed using a form of the model developed by Muzychka and Yovanovich [25] formulated as:

$$f_{\text{app}} = \frac{\sqrt{\left(\left(\frac{3.44}{\sqrt{L^*}} \right)^2 + \left(f \cdot \text{Re}_{D_h} \right)^2 \right)}}{\text{Re}_{D_h}} \tag{4.35}$$

where $L^* = \frac{L}{\text{Re}_{D_h} D_h}$, $\text{Re}_{D_h} = \frac{V_{ch} D_h}{\nu}$, $D_h = 2b$ and $f \cdot \text{Re}_{D_h}$ is the fully developed flow friction factor Reynolds number group given by:

$$f \cdot \text{Re}_{D_h} = 24 - (32.53 \cdot \lambda) + (46.72 \cdot \lambda^2) - (40.83 \cdot \lambda^3) + (22.95 \cdot \lambda^4) - (6.09 \cdot \lambda^5) \tag{4.36}$$

To determine the operating point of the fan and heat sink, an equilibrium with equations (4.32) and (4.33) is established, giving the volume flow rate as a function of the pressure drop at the heat sink.

$$\Delta P_{\text{fan}}(\dot{V}) - \Delta P_{\text{hs}}(\dot{V}) = 0 \tag{4.37}$$

Chapter 5

Validation

After modeling each component with the correct approaches, they will be implemented in an entire model using previously developed headlamp designs that incorporate different light modules, fans and airflow directions. Combining all components with a comprehensive system model can help better understand thermal performance and how various components interact. Simulating these existing headlamp models will show how accurate the 1D modeling is compared to CFD results. This comparison will enable the optimization of the system design to achieve the desired goals in terms of temperature.

The first three models to be evaluated have particular characteristics in internal structure. These models contain a single fan and a central light called the BiMatrix module (for high and low beam) and 5 PCBs. BiMatrix is composed of a circuit board with LED chips integrated into a control unit with a heat sink. Those five extra PCBs fulfill other functions: additional high beam, daytime running light, position light, direction indicator, and cornering light. The difference between these first three lamps lies in the position of the PCBs and the fan, which affects the airflow direction and influences the thermal behavior, see Figure 5.1. Additionally, the size of the lamps and the proportions between the housing and the cover lens are also relevant for simulations under two different temperatures.

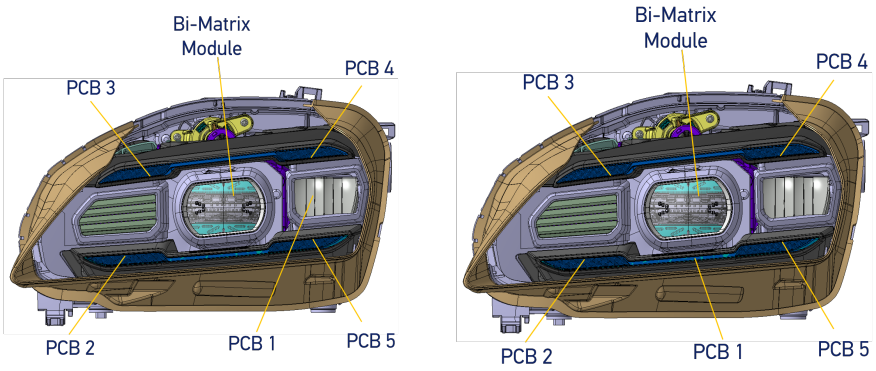

Figure 5.1: PCBs position (Left: Headlamp 1, Right: Headlamp 2 and 3) [14]

5.1 Modelica Representation

Headlamp 1 model, depicted in Figure 5.2, features a primary light module named BiMatrix (low beam and high beam) with a heat sink and five distinct PCBs. The fan drives the air upwards within a closed air guide where the heat sink of the light module is located, as shown in Figure 5.2. The duct directs air to five distinct PCBs. Following the cooling of these PCBs, most of the air is directed towards the front (cover lens) to enhance cooling, while a portion is also directed towards the rear (housing) because of

the internal structures. A robust representation has been developed in Modelica for better visualization of the system, where the initial point is considered at the fan. Subsequently, the air will pass between the fins of the heat sink, heating up due to the thermal power emitted by the LED. This hot air will then be directed toward the 5 PCBs that need to be equally cooled, which do not have heat sinks. At the end of this process, all the hot air would be dispersed towards the cover lens and housing in order to cool down before completing a closed cycle by being redirected to the fan.

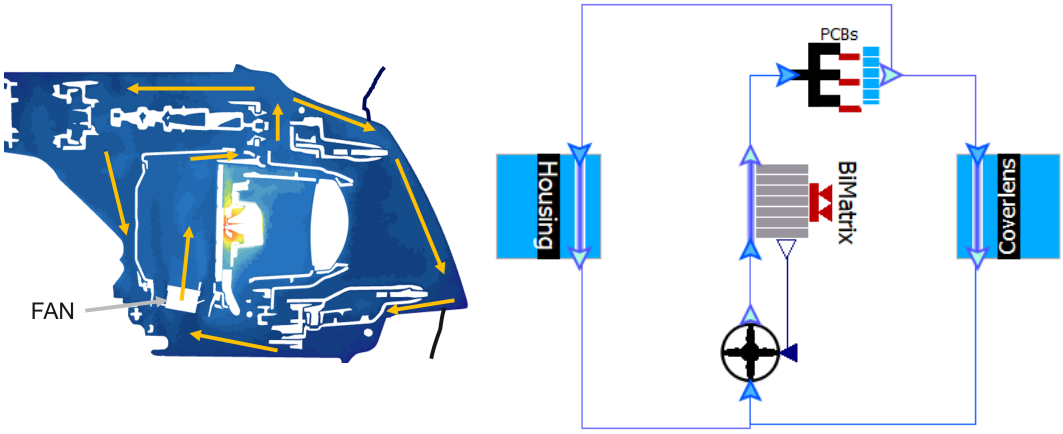

Figure 5.2: Headlamp 1 system overview and representation in Modelica

The second and third headlamp models, depicted in Figures 5.3 and 5.4, are also composed of a primary light module named BiMatrix (low beam and high beam) with a heat sink and five distinct PCBs, but in different positions compared to the first model. Two PCBs are at the top and the other three are at the bottom. For a better understanding, Modelica representation shows the airflow direction and how the fan position affects the cooling. Unlike the first model, the fan, located underneath the heat sink as the starting point, directs the air downward this time. This air is then conducted to cool PCBs 1, 2, and 5. Afterward, as the air is diverted forward and backward, rising along the sides, it manages to converge again to cool PCBs 3 and 4 and then enters into a guide towards the heat sink. Passing through the heat sink's fins, this air collects all the thermal power, cools the light module, then passes through the fan again, accelerating the airflow speed.

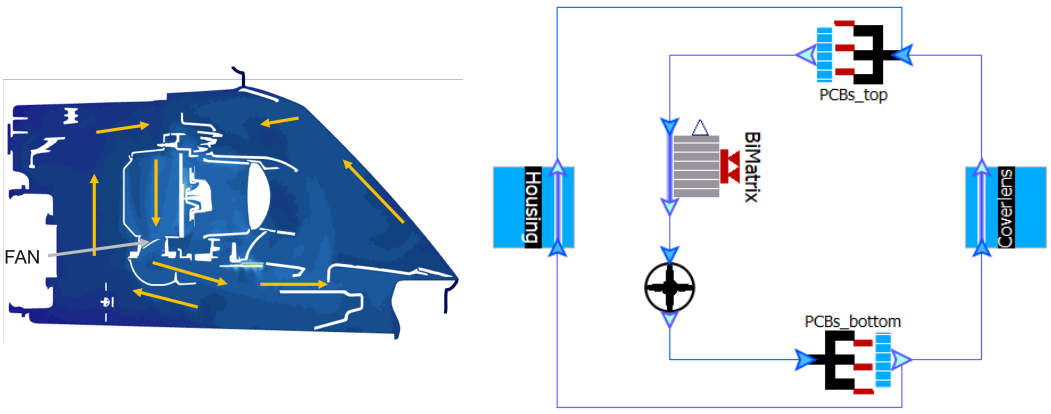

Figure 5.3: Headlamp 2 system overview and representation in Modelica

The third model has the same internal structure and airflow direction as Headlamp 2, as shown in Figure 5.4. The difference is that the air in contact with the housing has a direct shortcut to the heat sink without contact with the PCBs on the top part. Notably, the proportion between the housing area and the cover lens area is much smaller, playing an important role when the rear temperature is warmer than the front

temperature and affecting the airflow distribution in contact with either the housing or the cover lens.

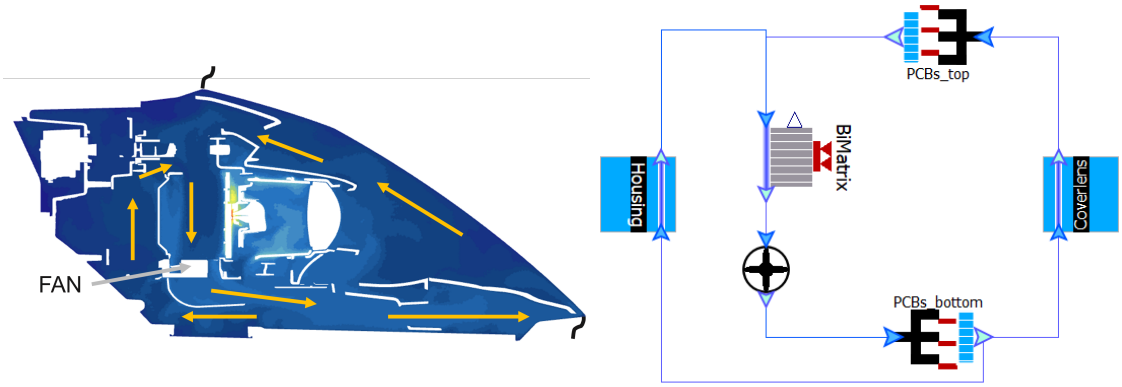

Figure 5.4: Headlamp 3 system overview and representation in Modelica

5.2 Data Inputs

Geometry Inputs

For the modeling, the component "Housing" includes the housing and the black cover lens (CL black). The component "Coverlens" includes the transparent cover lens (CL clear) and is the visible part of the headlamp from the outside. It tends to be a flat plate with a degree of inclination. See Figures 5.2, 5.3 and 5.4 to notice the differences in the clear cover lens. This division is helpful because, for some tests, the housing part is exposed at a different temperature than the cover lens as the chassis covers them, and its surrounding temperature is affected by the engine's heat, specifically in the "High-Temperature" test. The housing and cover lens parameters are listed in Table 5.1 below.

Parameter	Symbol	Housing	CL clear	CL black	Unit
Density	ρ	1200	1190	1200	kg/m^3
Thermal Conductivity	k	0.20	0.18	0.20	W/mK
Specific Heat	c_p	900	900	900	J/kgK
Thickness	th	2.7	2.6	2.7	mm
Area HL 1	A_1	0.262	0.049	0.094	m^2
Area HL 2	A_2	0.450	0.101	0.090	m^2
Area HL 3	A_3	0.255	0.114	0.058	m^2

Table 5.1: Headlamp skin parameters

Light Module Inputs

In these three headlamp models, the presence of a heat sink is unique to the BiMatrix due to its high thermal power. Understanding the parameters associated with the heat sink's design is pivotal, as they serve as inputs for calculating both the heat transfer coefficient and the pressure drop. The heat sink's geometrical parameters and material properties are included in Table 5.2 and Table 5.3.
For this model, the CFD simulation delivered the following temperatures at different points in the headlamp. These results will be compared with the results from Modelica. The BiMatrix and the other PCBs generate heat as previously outlined in Section 3.1.2, with variations depending on the test case. Each test case determines the temperatures and light functions. For the "High-Temperature" test, the BiMatrix module and PCBs are turned on, while in "Type-Approval" test, only the BiMatrix and PCB 1. The

L [mm]	W [mm]	H [mm]	d [mm]	b [mm]	t [mm]	N
65	75	50	3	5	0.5	14

Table 5.2: Heat sink geometrical parameters

Parameter	Symbol	Base plate	Fins	Unit
Density	ρ	2700	2660	kg/m^3
Thermal Conductivity	k	237	140	W/mK
Specific Heat	c_p	960	900	J/kgK

Table 5.3: Heat sink material properties

constant heat flow rate $\dot{Q}_{\text{in}}$ is provided as a parameter within a component. This parameter indicates a specific heat flow rate to be "injected" into a thermal system at a designated port. In the following Tables 5.4 and 5.5, the thermal power of BiMatrix and each PCB is given in two different test cases, at 25/25 ℃ and 75/35 ℃.

Light function	Headlamp 1	Headlamp 2	Headlamp 3
BiMatrix Low Beam	10.3 W	11.4 W	12.1 W
BiMatrix High Beam	8.6 W	9.1 W	8.5 W
PCB 1	1.8 W	4.6 W	-
PCB 2	-	0.2 W	0.1 W
PCB 3	-	0.2 W	0.1 W
PCB 4	-	0.2 W	0.1 W
PCB 5	-	0.2 W	0.1 W
Total	20.7 W	25.9 W	21.0 W

Table 5.4: Thermal power of the light functions in "Type-Approval" test

Light function	Headlamp 1	Headlamp 2	Headlamp 3
BiMatrix Low Beam	10.3 W	11.4 W	12.1 W
BiMatrix High Beam	7.1 W	9.1 W	8.5 W
PCB 1	1.8 W	4.6 W	4.6 W
PCB 2	0.5 W	0.2 W	0.1 W
PCB 3	0.5 W	0.2 W	0.1 W
PCB 4	0.7 W	0.2 W	0.1 W
PCB 5	0.7 W	0.2 W	0.1 W
Total	21.6 W	25.9 W	25.6 W

Table 5.5: Thermal power of the light functions in "High-Temperature" test

Test Case Inputs

Since the clear cover lens tends to be a vertical wall, the Nusselt correlation can help determine the heat transfer coefficient. In the CFD simulations based on Figure 3.13, free convection is observed around the headlamp's exterior, while forced convection occurs inside due to the fan. Turbulent airflow is evident in the simulation's airflow vectors, resulting from the headlamp's diverse internal geometries. Therefore, the natural convection approach calculates the outer heat transfer coefficient, while the forced convection approach is applied to determine the inner heat transfer coefficient. The equation (4.19) will be implemented to calculate the Nusselt number for inner convection and the equation (4.11) for the

outer convection. After the Nusselt number, the equation (4.20) will be applied to calculate the heat transfer coefficient for each "convection" component, as observed in Figure 4.3.

Because of the complex geometry of the housing and black cover lens in 1D modeling (horizontal and vertical plates) and the lack of information to calculate the velocities near the housing, the Nusselt correlation is not suitable here. Therefore, heat transfer coefficients for the component "Housing" are provided as inputs.

Parameter	Symbol	Housing	Coverlens	Unit
Area	A	H+CLB	CLC	m^2
Characteristic length	L_c	-	$(A/2)^{0.5}$	m
Partial volume flow	v_i	30	70	%
Inner heat transfer coefficient	α_{in}	6	Nu(Re, Pr)	W/m^2K
Outer heat transfer coefficient	α_{out}	5	Nu(Ra, Pr)	W/m^2K
Air velocity	u_{air}	-	0.5 for HL1, 0.3 for HL2/HL3	m/s

Table 5.6: Data for the component parameters in "Type-Approval" test

To simulate the thermal behavior in this scenario, the entire surface of the housing is exposed at 75 °C, representing the influence of the engine's heat, while the cover lens front is in contact with 35 °C, as the chassis does not cover it. As explained previously, forced convection at the outer cover lens and housing surface is presented in "High-Temperature" test. The equations (4.19) and (4.18) provide the heat transfer coefficients for inner and outer convection at the cover lens, respectively. The air velocities are average values obtained in the CFD simulation in order to get an accurate Reynolds number. The heat transfer coefficients for the housing are higher outside of the headlamp due to higher velocities.

Parameter	Symbol	Housing	Coverlens	Unit
Area	A	H+CLB	CLC	m^2
Characteristic length	L_c	-	$(A/2)^{0.5}$	m
Partial volume	v_i	30	70	%
Inner heat transfer coefficient	α_{in}	11	Nu(Re, Pr)	W/m^2K
Outer heat transfer coefficient	α_{out}	11	Nu(Re, Pr)	W/m^2K
Inner air velocity	$u_{air,\ in}$	-	0.5 for HL1, 0.3 for HL2/HL3	m/s
Outer air velocity	$u_{air,\ out}$	-	0.9	m/s

Table 5.7: Data for the component parameters in "High-Temperature" test

5.3 Results

In this section, the results obtained in Modelica are compared with those from previously conducted CFD simulations to evaluate the accuracy of the modeling. The required temperature is the LED temperature, but for a better understanding, an evaluation of other important temperatures located at different points, such as the fan temperature as an average of the internal air temperature, as well as the temperature of the heat sink to assess the accuracy of the heat transfer coefficient and the PCB temperature to evaluate the conductive heat transfer from the PCB to the fins. Focusing on the early development stage, the required LED temperature in Modelica must stand within a range of ±5 °C compared to the CFD results for the modeling to be considered valid.

5.3.1 Volume Flow

The fan's volume flow rate is a crucial parameter in various calculations for the heat transfer coefficient and boundary heat flux across the housing and cover lens. To calculate the volume flow, the equations of the section 4.3.3 will be applied, where, in this case, the pressure drop of the heat sink will be equal to the fan pressure drop because it is challenging to determine the pressure drop across the entire system, including the housing and the cover lens, due to internal geometries that disrupt the airflow and a lack of actual data about the shell geometry. Therefore, only the pressure at the heat sink was considered to determine the volume in the fan characteristic curve. This approach results in a higher volume flow value in Modelica, as shown in Figure 5.5.

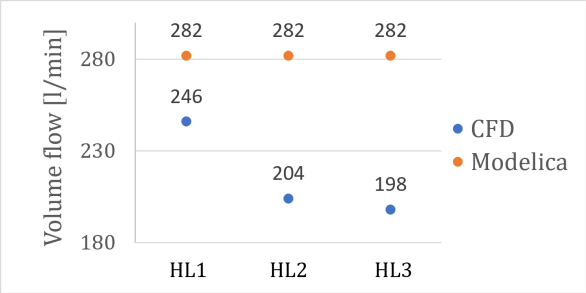

Figure 5.5: Comparison of the volume flow rate

In Modelica, the volume flow value is 0.0047 m^3/s (282 l/min) for the first three headlamps due to the exact geometrical measurements of the heat sink, while in CFD, the value obtained for the headlamp 1 is 0.0041 m^3/s (246 l/min). The volume flow rates for Headlamps 2 and 3 are 0.0034 m^3/s (204 l/min) and 0.0033 m^3/s (198 l/min), respectively. In Headlamp 1, the difference is relatively low due to the small size of the lamp, affecting the temperature at 1 °C. As the total pressure drop in the system is not considered, a big difference in volume flow values can be noticed in headlamps with high volume, as in headlamps 2 and 3, where the Modelica value modifies the temperature by 2.5 °C–3 °C.

5.3.2 Partial Volume Flow

As observed in Tables 5.6 and 5.7, there is a parameter called "Partial volume flow" that represents how much air flows towards the front (cover lens) or to the rear (housing). The headlamp's internal structure determines the exact partial volume value. However, the challenge here is that the data regarding the internal structure is unknown in the early development phase. This stage focuses mainly on meeting robust customer requirements, such as the number of fans or light modules and the positioning of certain PCBs. Therefore, with this lack of data, it is needed to adjust this parameter and understand its influence on the final LED temperature and how much it varies, as shown in Figure 5.6.

It is observed that the temperature increases as the airflow to the cover lens increases due to the smaller surface area compared to housing, leading to limited heat transfer to the ambient. However, there is a limit to this effect, especially in the "High-Temperature" test, where the housing is exposed to higher temperatures than the cover lens. Figure 5.6 shows that from 50% to 85% airflow, the variation lies between ±5 °C. However, different simulations show that the optimal values for minimizing deviation are between 65% and 80%. From 85% to 95%, the temperature increases radically to high temperatures. Compared to reality, there is always a focus on maximizing airflow towards the cover lens due to fogging issues and better cooling in driving cases, which have not yet been implemented in this modeling due to the complexity of representing the wind movement effect on the heat transfer accurately.

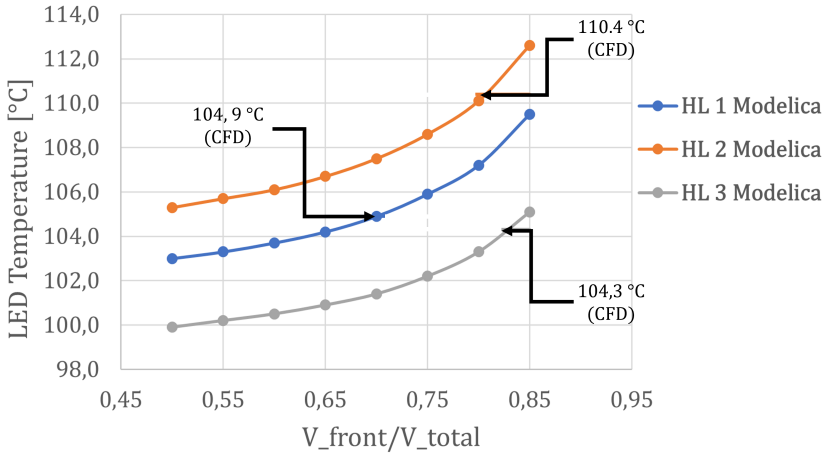

Figure 5.6: Influence of the volume distribution parameter on the temperature

5.3.3 Headlamp 1

Table 5.8 displays the relevant temperatures. Analyzing the LED temperature results for "Type-Approval" test, the Modelica temperature is the same as in CFD, while in the "High-Temperature" test, it is slightly higher than CFD. As explained in Section 3.3.3, there is forced convection for the "High-Temperature" test due to the airflow inlets in the climate chamber. In contrast, there is free convection in "Type-Approval" test, whose approach provides a more accurate heat transfer coefficient by not requiring air velocity. In forced convection, air velocity is required. It varies at each point of the headlamp, so when choosing an average velocity, there is a variation in the accuracy, giving a higher temperature in the second test. In Modelica, the aim is to always work with an average temperature for the air and a maximal temperature for the PCBs and LEDs, ensuring that it does not exceed their maximal working temperature.

	Type-Approval test			**High-Temperature test**		
	$T_{\text{front}} = 25°C, \quad T_{\text{rear}} = 25°C$			$T_{\text{front}} = 35°C, \quad T_{\text{rear}} = 75°C$		
	CFD	Modelica	Error	CFD	Modelica	Error
$T_{\text{air, fan}}$	45.1 °C	45.9 °C	1.7%	80.0 °C	82.6 °C	3.3%
$T_{\text{HS, BiMatrix}}$	61.5 °C	61.2 °C	-0.5%	95.3 °C	96.6 °C	1.4%
$T_{\text{PCB, BiMatrix}}$	98.4 °C	98.4 °C	-0.0%	125.0 °C	126.3 °C	1.1%
$T_{\text{LED, BiMatrix}}$	104.9 °C	104.9 °C	-0.0%	130.3 °C	131.6 °C	1.0%

Table 5.8: Temperature values of the light module in Headlamp 1

Now, analyzing each temperature, a higher temperature for the fan is given by Modelica in both tests, representing an average internal air temperature within the lamp. The fan temperature represents the air temperature before entering the heat sink (connected to the PCB). The test results indicate that the fan temperatures are higher than the CFD ones, but the temperature difference between the air leaving the fan and the heat sink in Modelica is smaller than in CFD due to a higher heat transfer coefficient in Modelica. The higher calculated volume flow rate in Modelica, as explained earlier, is the reason why a higher heat transfer coefficient is obtained in Modelica compared to CFD, giving a lower temperature at heat sink fins.

Another reason for a lower $T_{\text{HS,BiMatrix}}$ value is $R_{\text{th,baseplate}}$. The heat sink temperature reported in Table 5.8 refers to the temperature of the base plate side, which is in contact with the PCB. In CFD, the temperature difference of the base plate $\Delta T_{\text{baseplate}}$ is 0.55 °C, resulting in a thermal resistance $R_{\text{th,baseplate}}$ of 0.0291 K/W. On the other hand, the analytical approach $R_{\text{th,cond}}$ with the equation 4.2 calculates a thermal resistance $R_{\text{th,baseplate}}$ of 0.0026 K/W, giving a relatively small temperature difference $\Delta T_{\text{baseplate}}$

of 0.05℃. This is because, in the analytical approach, it is assumed that the heat flux density will be the same across the entire area of the heat sink base plate. However, in reality, the heat is not evenly dispersed, and most of it stays in the middle of the entire surface (where the LED is located), resulting in a higher temperature difference.

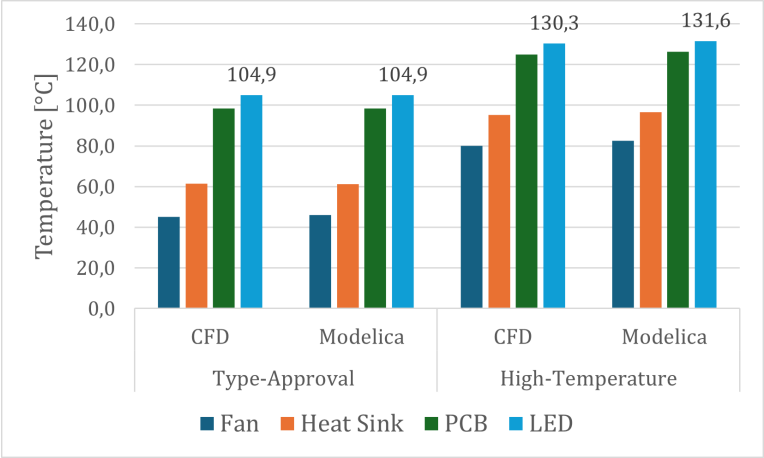

Figure 5.7: Comparison of the temperature values in Headlamp 1

In Table 5.4, it is observed that PCB 1 generates a thermal power of 1.78 W, heating both its temperature and the internal air temperature. As shown in Table 5.9, PCB 1 has a temperature $T_{\text{PCB, 1}}$ of 76.3 ℃ from CFD, while in Modelica, the temperature $T_{\text{PCB, 1}}$ = 76.0 ℃. The temperature was calculated by determining the air guide's volume flow rate and outlet area, first finding the air velocity and then the PCB characteristic length. Talking about the other PCBs without heat sinks, since they are not powered on (meaning that no heat transfer occurs), they take the surrounding air temperature, resulting in a similar temperature. The temperature obtained from Modelica is observed to be higher than that of CFD. This happens because this 1D modeling provides a single average air temperature after the heat sink. This average temperature is then applied to all PCBs, meaning that when they are not powered on, they all take the same air temperature. In contrast, in 3D modeling, different temperatures are managed at different points after the heat sink, and each airflow can vary in temperature depending on its location. In the "High-Temperature" test presented, the result for PCB 1 was accurate, while it was observed that the temperatures of the other PCBs showed a higher percentage of error compared to the CFD results. This error is because our calculation only considered the airflow exiting the air guide, while the PCBs are exposed to air flows with varying temperatures within the headlamp. As a result, a lower temperature was obtained in CFD than in Modelica.

	Type-Approval test			**High-Temperature test**		
	CFD	Modelica	Error	CFD	Modelica	Error
$T_{\text{PCB, 1}}$	76.3℃	76.0℃	-0.4%	110.0℃	112.2℃	2.0%
$T_{\text{PCB, 2}}$	47.0℃	48.7℃	3.6%	88.0℃	96.5℃	9.7%
$T_{\text{PCB, 3}}$	46.0℃	48.7℃	5.9%	88.0℃	97.1℃	10.3%
$T_{\text{PCB, 4}}$	46.0℃	48.7℃	5.9%	88.0℃	90.5℃	2.8%
$T_{\text{PCB, 5}}$	46.0℃	48.7℃	5.9%	88.0℃	105.3℃	19.7%

Table 5.9: PCBs temperature values in Headlamp 1

The calculation of heat transfer coefficients for the PCBs could be more precise. However, due to the need for more information on airflow behavior, including velocities and temperatures at different positions, more than a 1D model is needed to represent the whole air movement inside the headlamp. For PCB 1, an accurate result was obtained due to its position just after the outlet guide, receiving all the air at high

speed, resulting in an accurate value. After several attempts to achieve more accurate results for the other PCBs, it can only be concluded that their temperature results can be considered valid when PCBs are not powered on since they take on the value of the surrounding temperature.

5.3.4 Headlamp 2

In "Type-Approval" test, a much lower LED temperature is obtained in Modelica than in CFD because the volume flow used is higher in Modelica than in CFD, as explained in the previous section. Despite having an equal fan temperature, the temperature in the heat sink is much lower in Modelica because the air velocity increases with a higher volume flow, thereby increasing the heat transfer coefficient. The volume flow and the heat transfer coefficient play a crucial role here. If the volume flow is reduced to that of CFD, all temperatures will increase, including that of the fan. It is important to note that the fan temperature is a reference internal air temperature at that point, but there might be a portion of air with a higher temperature. This Modelica fan temperature, observed across different simulations, is usually higher than the CFD temperature due to simplifications in the external geometry (housing and cover lens) and internal structure (affecting airflow and velocity) changing the heat transfer.

	Type-Approval test			**High-Temperature test**		
	CFD	Modelica	Error	CFD	Modelica	Error
$T_{\text{air, fan}}$	49.1 °C	49.5 °C	0.8%	82.7 °C	84.1 °C	1.7%
$T_{\text{HS, BiMatrix}}$	65.1 °C	62.2 °C	-4.7%	99.1 °C	97.1 °C	-2.1%
$T_{\text{PCB, BiMatrix}}$	103.5 °C	100.6 °C	-2.9%	114.1 °C	112.4 °C	-1.5%
$T_{\text{LED, BiMatrix}}$	110.4 °C	107.5 °C	-2.7%	120.4 °C	118.9 °C	-1.3%

Table 5.10: Comparison of the temperature values in Headlamp 2

In the second test, the Modelica simulation shows a lower LED temperature. This happens because of two main factors: firstly, the higher volume flow rate increases the heat transfer coefficient. Secondly, there is a minor variation in the $T_{\text{air, fan}}$ values, which represents an average value of the internal air temperature at that point (compared to the $T_{\text{air, fan}}$ values in Headlamp 1 and Headlamp 3). These two factors result in a lower temperature in the heat sink. The small difference in the $T_{\text{air, fan}}$ results is due to the large volume of the lamp, which increases the surface area in contact with the ambient, leading to better cooling. Additionally, forced convection further contributes to this effect.

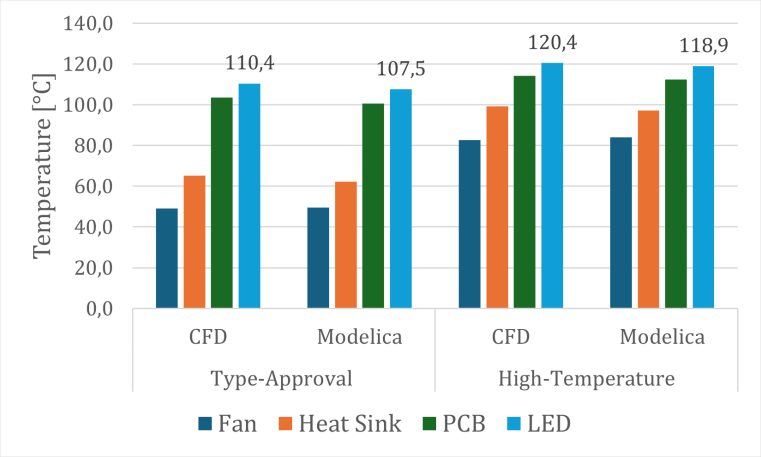

Figure 5.8: Comparison of the temperature values in Headlamp 2

5.3.5 Headlamp 3

As in Headlamp 1, the average air temperature is higher than the CFD value (referring to the fan temperature), but a lower temperature is obtained in the LED. This variation occurs because the Modelica volume flow value is used, which generates a higher heat transfer coefficient, thereby reducing the temperature in the heat sink and progressively towards the LED. In the event that the CFD volume flow value is used, the LED temperature would increase by 2 degrees. It is important to remember that the fan reference temperature is an average temperature; in Modelica, this is higher due to the various simplifications made to represent the heat transfer with the housing.

	Type-Approval test			**High-Temperature test**		
	$T_{\text{front}} = 25°\text{C}, \quad T_{\text{rear}} = 25°\text{C}$			$T_{\text{front}} = 35°\text{C}, \quad T_{\text{rear}} = 75°\text{C}$		
	CFD	Modelica	Error	CFD	Modelica	Error
$T_{\text{air, fan}}$	48.0 °C	50.1 °C	4.2%	78.9 °C	86.3 °C	8.0%
$T_{\text{HS, BiMatrix}}$	66.2 °C	63.9 °C	-3.6%	98.6 °C	100.1 °C	1.5%
$T_{\text{PCB, BiMatrix}}$	97.9 °C	95.1 °C	-2.9%	129.1 °C	130.6 °C	1.2%
$T_{\text{LED, BiMatrix}}$	104.3 °C	101.4 °C	-2.9%	135.5 °C	137.0 °C	1.1%

Table 5.11: Comparison of the temperature values in Headlamp 3

Regarding the "High-Temperature" test, there is a notable difference in $T_{\text{air, fan}}$. The outer geometry of the headlamp can explain this difference. Figure 5.4 shows a lateral cross-section of the lamp, where it can be observed that the cover lens has a large surface area and is inclined at a significant angle. This inclination affects the heat transfer in natural and forced convection, as the cover lens surface is exposed to different air flows with varying velocities and temperatures compared to a vertical plate. However, due to the complexity of modeling those characteristics, some simplifications were conducted to represent this heat transfer. As a result, Modelica gives a higher internal temperature, which can be seen in the fan temperature ($T_{\text{air, fan}}$). As explained earlier, the difference will be reduced for the LED temperature because of the higher volume flow and the thermal conduction from the PCB to the heat sink's fins.

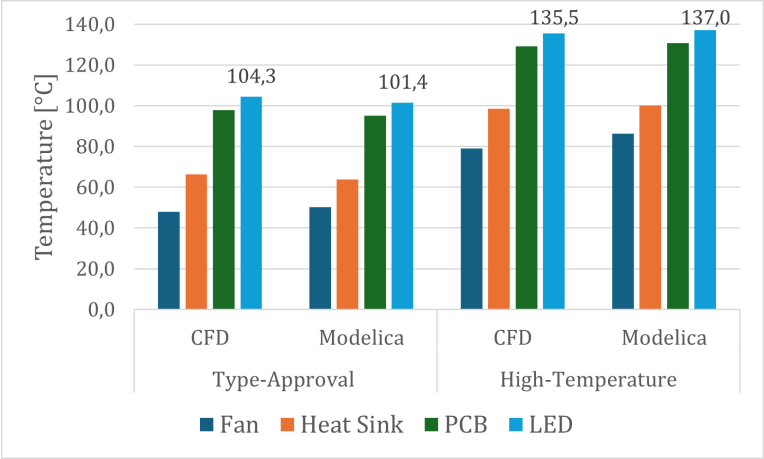

Figure 5.9: Comparison of the temperature values in Headlamp 3

Chapter 6

Validation for another internal structure

Previously achieved is modeling lamps with a similar internal structure, with one fan and one central light module. However, aiming to apply all the components developed from the basic model to a model with a more complex internal structure, such as more heat sinks and fans, to see if the modeling achieves a good level of accuracy. This headlamp, called Headlamp 4, has the same external geometry as Headlamp 1, with the same shape, surface area, and volume. The difference lies in the internal structure. Two fans and four main light modules have been implemented, as well as four PCBs for extra light functions.

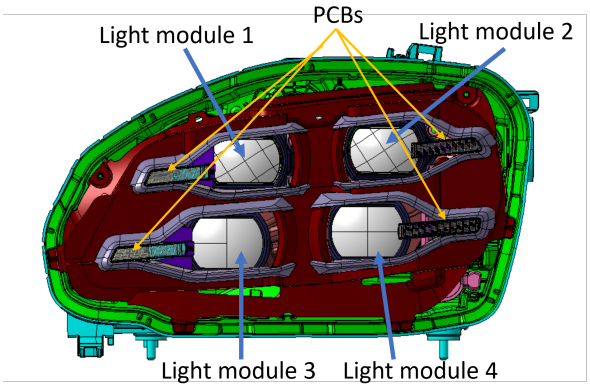

Figure 6.1: System overview of Headlamp 4 [14]

6.1 Modelica Representation

As previously mentioned, this lamp model has a more complex internal structure. For better understanding, each light module (LM) has its own function, such as high beam, low beam and prefield. LM 1 and LM 3 are on the left side, while LM 2 and LM 4 are on the right. Fan 1 is between LM 1 and LM 3, and Fan 2 is between LM 2 and LM 4, as shown in Figure 6.2.

The fans are positioned between two heat sinks of light modules to direct air downward. Consequently, the fans drive two streams at different volume flow rates through the heat sink fins. The PCBs are in contact with the mixed air after the heat sinks, dividing it into the cover lens and housing sides. Then, the air moves up near the housing and cover lens towards the upper side, splitting the air into two streams that cool the first light modules.

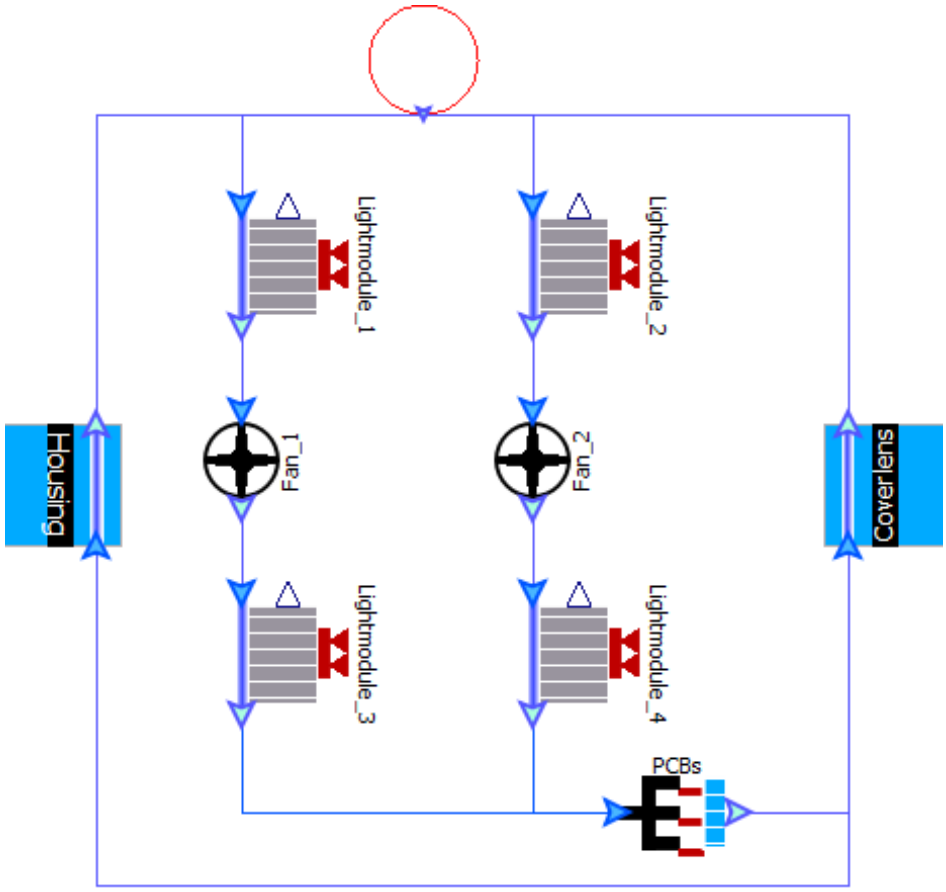

Figure 6.2: Modelica representation of Headlamp 4

6.2 Data Inputs

From section 5.2, the geometry inputs from Headlamp 1 and the test case inputs for the "Type-Approval" and "High-Temperature" tests will be taken to simulate Headlamp 4. What differs are the sizes of the heat sinks and the thermal powers of the different light functions. In this headlamp model, each light module has a heat sink due to high emitted thermal power. The heat sink's geometrical parameters and material properties for each light module are included in Table 5.2 and Table 5.3. As observed, all heat sinks have the same material properties, but the geometrical parameters of the heat sinks differ between the top and bottom.

	L [mm]	W [mm]	H [mm]	d [mm]	b [mm]	t [mm]	N
LM1 - LM2	50	70	20	3	5	0.5	12
LM3 - LM4	65	65	35	4	5	0.1	14

Table 6.1: Geometrical parameters of the heat sinks in Headlamp 4

Parameter	Base plate	Fins	Unit
Density	2700	2660	kg/m^3
Thermal Conductivity	237	140	W/mK
Specific Heat	960	900	J/kgK

Table 6.2: Material properties of the heat sinks in Headlamp 4

The four light modules and the other PCBs generate heat with variations depending on the test case.

The temperatures and light functions are determined by each test case. For the "High-Temperature" test, the main light modules and PCBs are turned on, while in the "Type-Approval" test, only the main light modules are turned on. In the next two tables, the thermal power of light modules and PCBs is given in two different test cases, at 25/25 °C and 75/35 °C.

Light function	Type-Approval test	High-Temperature test
Light module 1	12.2 W	4.2 W
Light module 2	12.2 W	4.2 W
Light module 3	25.5 W	11.9 W
Light module 4	23.2 W	11.1 W
PCBs	-	3.0 W
Total	73.1 W	34.4 W

Table 6.3: Thermal power of the light functions

6.3 Results

The results displayed in Table 6.4 indicate a reasonable margin of error in both the "Type-Approval" and "High-Temperature" tests. For the "Type-Approval" test, all components are tested at an ambient temperature of 25 °C. For the "High-Temperature" test, the housing is tested at an ambient temperature of 75 °C, except for the cover lens, which is exposed at 35 °C. There are different thermal powers of each test, varying by the required light functions. Knowing the fan's position is crucial in this case, as it influences the velocity in its proximity and airflow direction. In CFD, the volume flow rate is 0.0041 m^3/s (246 l/min) for Fan 1 and 0.003 m^3/s (180 l/min) for Fan 2 due to the position in the headlamp.

	Type-Approval test			**High-Temperature test**		
	$T_{front} = 25°C, \quad T_{rear} = 25°C$			$T_{front} = 35°C, \quad T_{rear} = 75°C$		
	CFD	Modelica	Error	CFD	Modelica	Error
$T_{air,\ fan\ 1}$	89.0 °C	90.1 °C	1.2%	90.0 °C	90.7 °C	0.7%
$T_{air,\ fan\ 2}$	84.0 °C	91.0 °C	7.7%	87.0 °C	91.0 °C	4.4%
$T_{HS,\ LM\ 1}$	99.2 °C	102.0 °C	2.7%	93.3 °C	94.7 °C	1.5%
$T_{PCB,\ LM\ 1}$	116.1 °C	118.9 °C	2.3%	101.9 °C	101.8 °C	-0.1%
$T_{HS,\ LM\ 2}$	92.5 °C	102.4 °C	9.7%	89.5 °C	94.9 °C	5.7%
$T_{PCB,\ LM\ 2}$	109.4 °C	119.3 °C	8.3%	98.1 °C	101.9 °C	3.8%
$T_{HS,\ LM\ 3}$	112.4 °C	109.2 °C	-2.9%	101.9 °C	99.6 °C	-2.3%
$T_{PCB,\ LM\ 3}$	117.9 °C	114.5 °C	-2.9%	104.3 °C	102.0 °C	-2.3%
$T_{HS,\ LM\ 4}$	110.3 °C	109.3 °C	-0.9%	99.9 °C	99.7 °C	-0.2%
$T_{PCB,\ LM\ 4}$	115.9 °C	114.9 °C	-0.9%	102.2 °C	102.2 °C	-0.2%

Table 6.4: Temperature values of the light modules and fans in Headlamp 4

First, analyzing the CFD values, the temperatures of the light modules on the left side (LM 1 and LM 3) are higher than those on the right side (LM 2 and LM 4) because LM 2 emits more thermal power than LM 4. However, different values are observed in Modelica. LM 1 and LM 2 have similar temperatures because Fan 2 has a lower volume flow, which influences the heat transfer coefficient. Clearly, in Figure 6.3, the temperatures of $T_{air,\ fan\ 1}$ and $T_{air,\ fan\ 2}$ obtained in Modelica are similar, while in CFD, $T_{air,\ fan\ 2}$ should be significantly lower than $T_{air,\ fan\ 1}$. This difference is also noted in the results of the light modules' temperatures, which is explained by the shell geometry and by the fact that in Modelica, there is a mixture of both air streams after the LM 3 and LM 4, dividing again for the cover lens and housing. After that, there is again a mixture of air, and the incoming temperature will be the same for both LM 1 and LM 2.

Since Fan 2 has a lower volume flow rate than Fan 1, the temperature in the heat sink and PCB of LM 2 and LM 4 will be slightly higher.

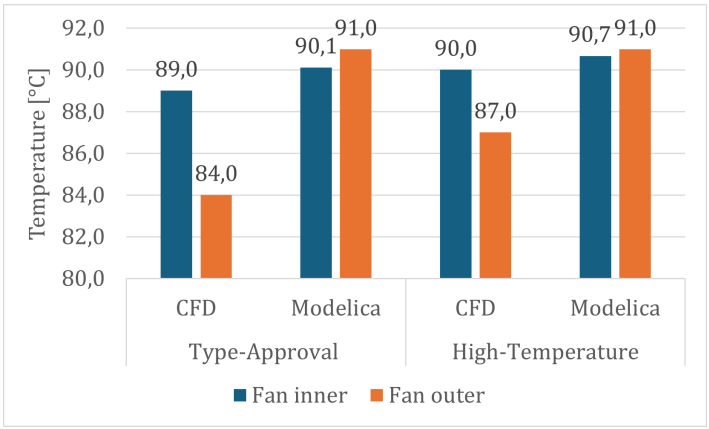

Figure 6.3: Comparison of the temperature values in the fans

In the CFD simulation, the air is not completely mixed, as the airflow takes different directions without complete mixing. The air enters at a higher velocity in LM2, as it has a shorter distance on the right side than the left side (a > b), enhancing the heat transfer coefficient (see in Figure 6.4). In Modelica, the volume flow of Fan 1 goes through the heat sinks' fins of LM 1 and LM 3, while Fan 2 gives the volume flow to LM 2 and LM 4. In CFD, this is not the case. Due to the internal structures, airflow suffers deviations, causing turbulence and affecting a continuous flow through the fins, consequently minimizing the heat transfer coefficient. The differences observed in temperature values between CFD and Modelica simulations could be partly attributed to discrepancies in accurately modeling the airflow behavior and accounting for turbulence effects. Detailed modeling of parameters, such as turbulence and boundary conditions, might help improve the results, but they are achieved in CFD simulations.

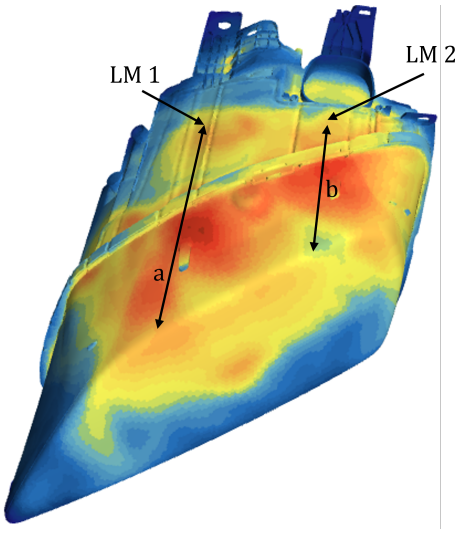

Figure 6.4: Outer geometry of Headlamp 4 [14]

In Figures 6.5 and 6.6, it is observed that in LM 2, $T_{\text{PCB, LM 2}}$ and $T_{\text{HS, LM 2}}$ have the highest difference in the temperature values and $T_{\text{air, fan 2}}$. In cases where two or more fans are implemented with different light modules and heat sinks, more than 1D modeling is needed to accurately represent the airflow behavior. The maximal operating temperature is, in most cases, 125 °C. The manufacturer of the LED technology provides this data. These variations result from factors such as the complexity of the geometry, assumptions, and simplifications made in the simulations, affecting the accuracy of the models used

in CFD and Modelica.

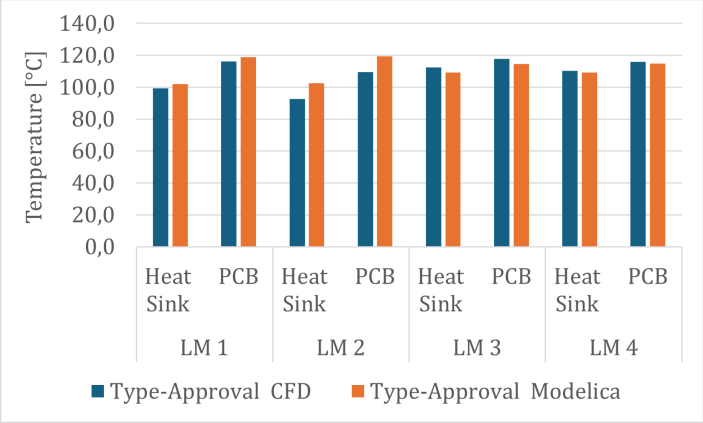

Figure 6.5: Comparison of temperature values in Headlamp 4 for "Type-Approval" test

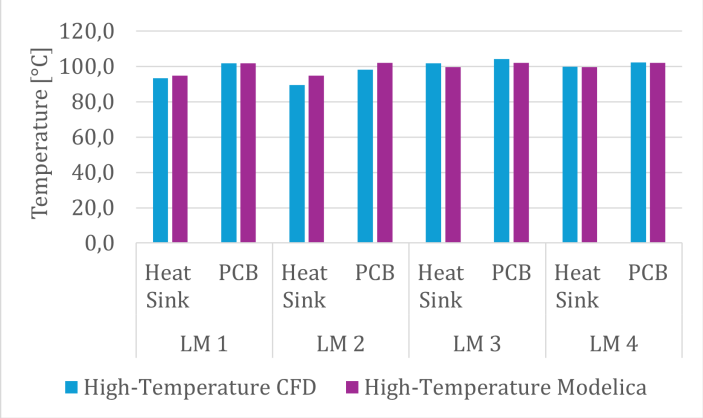

Figure 6.6: Comparison of the temperature values in Headlamp 4 for "High-Temperature" test

Chapter 7

Conclusion

This work aims to develop thermal modeling of headlamps by integrating the heat transfer processes inside a headlamp. The challenge is to find a suitable way to implement convective heat transfer and air movement in a thermal system with adequate accuracy.

A 1D model for heat transfer, including convection, is needed for a robust temperature prediction within a headlamp in the early development stage. The importance lies in understanding the environment to which the LED modules are exposed. As is known, they react very sensitively to heat, thereby affecting their lifetime and luminous efficacy at high temperatures. Therefore, they require an adequate thermal and cooling system, including heat sinks and fans inside the headlamp. Modeling the headlamp's thermal system helps analyze the thermal transfer and airflow behavior inside the headlamp. The reason for knowing the temperature data in the development phase is to fulfill customer requirements and prevent future failures of the LED module. This temperature data can also be used for other specialized modeling to predict the fogging and defogging behavior.

Before this work, the thermal system was modeled using a thermal network with resistances. The innovative aspect of this thesis is implementing a thermo-fluid model, adapting specific components already created in the OpenModelica libraries or creating new ones. Components such as the fan and convective heat transfer can be parameterized by including airflow along with thermal resistances. These parameters will help calculate the heat transfer coefficients, describe the heat transfer and calculate the temperature.

During the early stages of development, the lack of information on the internal and external geometry of the lamp leads to the challenge of replicating the airflow in a 1D model. Therefore, several simplifications in the complex geometry and airflow characteristics were made to calculate average heat transfer coefficients in different headlamp parts. Specifically, these simplifications include the thermal transfer between the heat sink and the air passing through the fins, the thermal transfer from the internal air to the ambient through the shell geometry, and the volume flow based on the heat sink pressure drop rather than the total pressure drop of the headlamp.

The developed modeling was validated by simulating four headlamp designs in Modelica to be compared with previously conducted CFD simulations to evaluate the accuracy of the 1D modeling. The first comparison of the results between CFD and Modelica helps address the accuracy of the temperature values between headlamps with different outer geometries but identical internal structures. Additionally, a headlamp with the same outer geometry but different internal structures was simulated to evaluate the accuracy of the modeling by adding more components (four light modules with heat sinks and two fans). The modeling also evaluates the precision of heat transfer coefficient calculations through analytical approaches.

During the modeling process, different approaches were explored to represent heat transfer for both the housing and cover lens. Due to its more complex geometry, the housing presents challenges in accurately determining the heat transfer coefficient. Given the challenge of accurately calculating the heat transfer coefficients in the developed model due to the reduction of the entire housing geometry, a new design analysis was developed but failed. This analysis involved discretizing each part for greater accuracy. Specifically, since the housing consists of two horizontal plates and two vertical plates on the sides, each part will undergo an analytical approach to determine the appropriate heat transfer coefficient. This spatial discretizing aimed to ensure that all the different methods for accurately calculating heat transfer were acceptable and that each shell part was implemented correctly. The discretization resulted in five parts with different velocities and areas, but the inputs needed to be known without conducting 3D simulations.

Therefore, the conclusion was that a universally applicable modeling with fewer inputs, known from the early development stage, should be further developed. Consequently, it was decided to provide these coefficients as inputs obtained from CFD. In the future, correlations should be established for each headlamp's heat transfer coefficient values. The author recommends using the values in the validation chapter 5.2, as they achieve high accuracy across all four lamps. In this case, Modelica results within a ±5 °C difference from the CFD values are achieved for the first three lamps. However, a significant percent error is observed for the temperatures of the PCBs without heat sinks. This error is due to their location, as they are exposed to different air flows at varying speeds and temperatures, making 1D modeling very complex. A more detailed modeling could be achieved, but the question is: up to what point does making the 1D modeling more detailed remain time-effective compared to CFD in order to replace it, or is it better to stick with a robust model and introduce a CFD simulation for an exhaustive thermal and climate analysis?

Another challenge was the volume flow because the only known variable was the pressure drop in the heat sink and not the whole headlamp pressure drop due to a lack of geometry. Therefore, the values obtained by Modelica suffer variations depending on the headlamp's geometry. However, the Modelica volume flow value only changes the final LED temperature at 2–3 °C. Regarding Headlamp 4, a more complex design problem arises where the light modules and fan positions influence the results. The error lies in the oversimplification of the airflow. The challenge is representing the airflow first in 2D and then in 3D modeling. Therefore, the results should be evaluated with the mentioned considerations for future simulations and compared with realistic values from other headlamp designs.

The developed simulation model enables a robust prediction of the temperature and airflow behavior in the headlamp, focusing on the early stages of the development process. Modeling each component identifies future issues in advance and optimizes the properties of each component. In this work, only the cooling concept of the Fin Heat Sink was modeled. However, Modelica offers the possibility of modeling other cooling concepts, such as heat pipe and water cooling using a cold plate, including a fluid flow analysis. The final comparison of the Modelica results with the CFD simulation results demonstrates that accurate modeling can be represented well, and the temperatures and flows in critical areas achieve reasonable accuracy. However, the results also show that the simulation model needs improvement for specific structures, like more fans and light modules with heat sinks.

Bibliography

[1] Lasance, C. and Poppe, A., eds. *Thermal Management for LED Applications*. New York: Springer, 2014.

[2] Brunberg, J. and Aspelin, M. “CFD Modelling of Headlamp Condensation”. MA thesis. Göteborg, Sweden: Chalmers University of Technology, 2011.

[3] Hämmerle, S. “Lifetime- and Economic Efficiency Simulation of LED Luminaires in Dymola/Modelica”. Master’s Thesis. FHV University of Applied Sciences, 2017.

[4] Mobedi, M. and Ilis, G. G. *Fundamentals of Heat Transfer: An Interdisciplinary Analytical Approach*. Springer, 2023.

[5] Çengel, Y. A. *Heat Transfer: A Practical Approach*. 2nd. McGraw-Hill, 2002.

[6] Ghoshdastidar, P. S. *Heat Transfer*. 2nd. Oxford University Press, 2012.

[7] Venkateshan, S. *Heat Transfer*. 3rd. Springer, 2021.

[8] Han, J. and Wright, L. M. *Analytical Heat Transfer*. 2nd. Taylor & Francis Group, 2022.

[9] Wördenweber, B., Boyce, P., Hoffman, D. D., and Wallaschek, J. *Automotive Lighting and Human Vision*. Berlin Heidelberg: Springer, 2007.

[10] Hella. *Hella Automotive Lighting*. Accessed on April 16, 2024. URL: https://www.hella.com/techworld/uk/Technical/Automotive-lighting/Headlights-219/.

[11] Teertstra, P. M., Yovanovich, M. M., Culham, J. R., and Lemczyk, T. F. “Analytical forced convection modeling of plate fin heat sinks”. In: *Proc. 15th Annu. IEEE Semicon. Thermal Meas. Manag. Symp.* San Diego, CA, 1999, pp. 34–41.

[12] Griesinger, A. *Wärmemanagement in der Elektronik: Theorie und Praxis*. Springer, 2019.

[13] Anderson Jr., J. D. *Computational Fluid Dynamics: The Basics with Applications*. 1997.

[14] Hella. *CFD simulation*. Accessed on April 16, 2024.

[15] Weiss Technik. *Scheinwerferprüfstand*. Accessed on April 16,2024. URL: https://www.weiss-technik.com/umweltsimulation/de/produkte/detail/scheinwerferpruefstand~p3865.

[16] Fritzson, P. *Principles of Object-Oriented Modeling and Simulation with Modelica 2.1*. Wiley-IEEE Press, 2004.

[17] Modelica Association. *Modelica - Home*. Accessed on April 11, 2024. URL: http://www.modelica.org.

[18] OpenModelica. *Modelica Thermal Library*. Accessed on April 16, 2024. URL: https://https://build.openmodelica.org/Documentation/Modelica.Thermal.html.

[19] Paul, A., Holy, F., Textor, M., and Lechner, S. “Experimentelle Untersuchung und numerische Modellierung eines sensiblen Hochtemperaturspeichers”. In: *12. Internationale Energiewirtschaftstagung an der TU Wien IEWT* (2021).

[20] Zimmer, D., Meißner, M., and Weber, N. “The DLR ThermoFluidStream Library”. In: *Proceedings of the 14th International Modelica Conference*. Modelica Association and Linköping University Electronic Press. Linköping, Schweden, 2021, pp. 225–234. ISBN: 978-91-7929-027-6. DOI: 10.3384/ecp21181225.

[21] e.V., V. *VDI Heat Atlas*. 2nd. Düsseldorf, Germany: Springer, 2010.

[22] Hüttemann, S. “Thermische Systemmodellierung eines LED-Scheinwerfers”. MA thesis. Bielefeld, Germany: FH Bielefeld, University of Applied Sciences, 2019.

[23] Lasance, C. J. M. “Heat Spreading: Not a Trivial Problem”. In: *Electronics Cooling* (May 1, 2008). URL: https://www.electronics-cooling.com/2008/05/heat-spreading-not-a-trivial-problem/.

[24] Culham, J. R. and Muzychka, Y. S. “Optimization of Plate Fin Heat Sinks Using Entropy Generation Minimization”. In: *IEEE Transactions on Components and Packaging Technologies* 24.2 (2001).

[25] Muzychka, Y. S. and Yovanovich, M. M. “Modeling friction factors in non-circular ducts for developing laminar flow”. In: *Proc. 2nd AIAA Theoretical Fluid Mech. Meeting*. Albuquerque, NM: AIAA, 1998.

Disclaimer

I hereby declare that this thesis is entirely the result of my own work except where otherwise indicated. I have only used the resources given in the list of references.

Garching, July 01, 2024

(Signature)